



LoRDO: Distributed Low-Rank Optimization with Infrequent Communication

Andrej Jovanović¹ Alex Iacob^{1,2} Mher Safaryan³ Ionut-Vlad Modoranu⁴ Lorenzo Sani^{1,2} William F. Shen¹
Xinchi Qiu¹ Dan Alistarh^{4,5} Nicholas D. Lane^{1,2}

Abstract

Distributed training of foundation models via DDP is limited by interconnect bandwidth. While infrequent communication strategies reduce synchronization frequency, they remain bottlenecked by the memory and communication requirements of optimizer states. Low-rank optimizers can alleviate these constraints; however, in the local-update regime, workers lack access to the full-batch gradients required to compute low-rank projections, which degrades performance. We propose LoRDO, a principled framework unifying low-rank optimization with infrequent synchronization. We first demonstrate that, while global projections based on pseudo-gradients are theoretically superior, they permanently restrict the optimization trajectory to a low-rank subspace. To restore subspace exploration, we introduce a full-rank quasi-hyperbolic update. LoRDO achieves near-parity with low-rank DDP in language modeling and downstream tasks at model scales of 125M–720M, while reducing communication by $\approx 10\times$. Finally, we show that LoRDO improves performance even more in very low-memory settings with small rank/batch size.

1. Introduction

Distributed optimization methods, such as DiLoCo (Douillard et al., 2023) and DES-LOC (Iacob et al., 2026b), have emerged as a solution to the substantial communication overheads inherent to Distributed Data Parallel (DDP) training. By leveraging local updates, these approaches reduce the bandwidth requirements for training large models.

However, the deployment of such methods faces *two critical constraints*. First, for large-scale training (Brown et al., 2020; Touvron et al., 2023; Dubey et al., 2024; DeepSeek-AI et al., 2025), the local optimization procedure on each

¹University of Cambridge ²Flower Labs ³Lancaster University, ⁴Institute of Science and Technology Austria ⁵Red Hat AI. Correspondence to: Andrej Jovanović <aj693@cam.ac.uk>.

Preprint. February 5, 2026.

worker incurs a significant memory overhead when storing optimizer momenta (Kingma & Ba, 2015; Pagliardini et al., 2025; Jordan et al., 2024), limiting the maximum trainable model size. Second, communicating optimizer states, required for convergence guarantees (Cheng & Glasgow, 2025), undermines the communication-efficiency gains of infrequent synchronization (Douillard et al., 2023).

Low-rank adaptive optimizers, such as GaLore (Zhao et al., 2024) and LDAdam (Robert et al., 2025), offer a path to alleviate the memory and communication bottlenecks of large-scale training. However, generalizing these methods to the infrequent-synchronization regime, while preserving guarantees, presents an optimization challenge. We show that computing low-rank projections locally on individual workers is detrimental; the reduced effective batch size per data shard introduces significant projection noise, resulting in a suboptimal projection subspace. While a global projection strategy, derived from the aggregated pseudo-gradient, can mitigate this noise and recover a stable basis analogous to DDP, we show that it introduces a critical failure mode: *it permanently constrains the optimization to a fixed rank- r subspace*. This rank restriction severely limits exploration, reducing final performance during training. To resolve this, we investigate the following design question:

How can we design high-performance low-rank optimizers for communication-efficient training?

To answer this, we propose LoRDO, a framework that adapts low-rank optimizers for distributed training with infrequent communication. Specifically, we demonstrate that injecting a full-rank quasi-hyperbolic momentum signal into each worker’s updates prevents stagnation of the global projection. This modification allows LoRDO to have near-parity with DDP and full-rank baselines while retaining the efficiency benefits of low-rank structures. Empirically, LoRDO reduces the communication overhead of low-rank DDP by $\approx 10\times$ at the 125M and 720M model scales. Despite these substantial reductions, LoRDO maintains near-parity with this baseline, exhibiting a negligible perplexity gap of less than 1% and matched downstream task accuracy. The contributions of our work are as follows:

Contributions :

- Analysis of projection failure modes.** We demonstrate that local projections harm performance due to high variance arising from small worker batch sizes, while global projections induce subspace stagnation.
- Restoring full subspace exploration.** We propose LORDO, a low-rank optimizer which injects a full-rank gradient signal into the local update while maintaining a global projection derived from the aggregated pseudo-gradient. This prevents stagnation without increasing communication/memory overheads.
- DDP parity and efficiency.** We show that LORDO achieves near-parity with synchronous low-rank DDP (perplexity gap < 1%) while reducing optimizer memory and communication by up to $8 \times - 12 \times$. Under heavy memory constraints, which necessitate low ranks, LORDO surpasses DDP by 3.36 – 4.7% in perplexity, while also demonstrating superior resilience to small-batch regimes compared to local projection methods.

2. Low-Rank Adaptive Optimization

As a motivating example, we describe low-rank optimizers using a single linear layer $W \in \mathbb{R}^{p \times q}$, a core component of Transformer models we use in Section 4. Consider training a model x with M workers. Using Adam, each worker m computes the following at time step t :

$$\begin{aligned} G_t^m &\leftarrow \nabla F(x_t^m; \xi_t^m) \\ u_t^m &\leftarrow \beta_1 u_{t-1}^m + (1 - \beta_1) G_t^m \\ v_t^m &\leftarrow \beta_2 v_{t-1}^m + (1 - \beta_2)(G_t^m \odot G_t^m) \\ x_{t+1}^m &\leftarrow x_t^m - \eta \frac{\hat{u}_t^m}{\sqrt{\hat{v}_t^m} + \epsilon} \end{aligned}$$

Each worker stores two optimizer states of size $O(pq)$, equal to the local gradient size. For large-scale models, this creates a significant memory bottleneck. Low-rank adaptive optimizers (Zhao et al., 2024; Robert et al., 2025) alleviate this by maintaining momenta in a projected low-rank form while allowing full solution exploration. Using a projection matrix $Q_t^m : \mathbb{R}^{p \times r}$, the update becomes:

$$\begin{aligned} g_t^m &\leftarrow (Q_t^m)^\top \nabla F(x_t^m; \xi_t^m) \\ u_t^m &\leftarrow \beta_1 u_{t-1}^m + (1 - \beta_1) g_t^m \\ v_t^m &\leftarrow \beta_2 v_{t-1}^m + (1 - \beta_2)(g_t^m \odot g_t^m) \\ x_{t+1}^m &\leftarrow x_t^m - \eta Q_t^m \left(\frac{\hat{u}_t^m}{\sqrt{\hat{v}_t^m} + \epsilon} \right). \end{aligned}$$

This regime reduces optimizer state memory overhead from $O(2pq)$ to $O(2r(p + q))$, where typically $r \ll p, q$.

To compute the projection matrix Q , Zhao et al. (2024) employ periodic SVD updates (Golub & Reinsch, 1970),

while Robert et al. (2025) use PowerSGD (Vogels et al., 2019) to estimate singular vectors at every step. An SVD projection in the DDP regime at step t for worker m is:

$$\begin{aligned} U, S, V &\leftarrow SVD(G_t^m) \\ Q_t^m &\leftarrow U[:, :r]. \end{aligned}$$

3. Designing LORDO

In this section, we describe the key design decisions behind LORDO, whose pseudocode is given in Algorithm 1. We first show that the global projection approach, while theoretically superior, can restrict learning to a stagnant subspace (see Section 5.1). LORDO adds a full-rank quasi-hyperbolic momentum term that restores full subspace exploration while realizing the initial theoretical benefits, bringing empirical improvements (Section 5.2). Additionally, we outline that aligned momenta (Robert et al., 2025) and error feedback (Seide et al., 2014) are essential for optimal performance, as ablated in Figures 6 and 7. Finally, we provide a discussion on the memory and communication benefits achieved by LORDO, which is elaborated further in Sections B.5 and B.6.

Notation. We consider standard distributed training settings with M workers, where each worker performs K local updates prior to synchronization. Training is conducted by minimizing a global objective function $f(x) := \frac{1}{M} \sum_{m=1}^M f_m(x)$ over the model parameters x , where each $f_m(x)$ is the local objective $\mathbb{E}_{\xi \sim \mathcal{D}_m}[F_m(x; \xi)]$, where the F_m is the local loss for a data sample ξ drawn from data distribution \mathcal{D}_m . Full derivations are provided in Section B.

3.1. LORDO Projection Matrices

In DDP, all workers use a shared projection matrix Q_t^m as gradients are synchronized across all workers prior to the optimizer step. However, in distributed optimization schemes such as those introduced in Douillard et al. (2023); Jacob et al. (2026b), parameter and optimizer state synchronization occurs only after K steps of local training. Adapting low-rank optimizers to the local-update regime is non-trivial as workers lack access to the full-batch gradients required to compute projection matrices Q_t^m as in DDP.

The naïve integration of low-rank optimizers into such frameworks is to allow each worker m to determine its own projection matrix Q_t^m locally based on its stochastic gradient G_t^m . However, we now discuss two issues related to this approach, which we resolve by the introduction of a global projection based on the aggregated pseudo-gradient.

Lack of Worker Unification. Since each worker determines its own projection matrix Q_t^m , workers are not guaranteed to optimize within the same basis, as each individual projection matrix could isolate an indepen-

Algorithm 1 LoRDO-Global - Bias Correction Omitted for Ease of Notation

Require: Model tensors, hyper-parameters

dent subspace. This causes interference upon aggregating the pseudo-gradients: $\sum_{m=1}^M \sum_{\tau=t-K}^t \eta_t^m Q_m^t \alpha_t^m \neq \bar{Q}_t \sum_{m=1}^M \sum_{\tau=t-K}^t \eta_t^m \alpha_t^m$ where \bar{Q}_t is the projection matrix that would have been obtained if using a gradient averaged across all workers as in DDP. While in the IID case, this may slightly lower final performance, for Non-IID data distributions, it may cause complete divergence.

Lower-Quality Projections. Assume that the stochastic gradient \hat{G} is a perturbed version of the true gradient G such that $\hat{G} = G + E$, where E represents the additive noise incurred through the stochastic sample (Bottou et al., 2018). Furthermore, we assume that the noise scales proportionally to $\frac{\kappa}{\sqrt{B}}$, where B is the batch size and κ is the variance of the

individual samples (McCandlish et al., 2018; Bottou et al., 2018). Additionally, as showed by Xie et al. (2023), we assume that the singular values of G and \hat{G} follow a power-law where $\sigma_r = Cr^{-\alpha}$ where $\alpha > 0$. Using the Davis-Kahan $\sin \Theta$ theorem (Stewart & Guang Sun, 1990; Davis & Kahan, 1970), we derive the instability of the projection matrix:

$$\Delta(\hat{Q}) \approx \frac{\kappa/\sqrt{B}}{\alpha C r^{-(\alpha+1)}} = \frac{\kappa}{\alpha C \sqrt{B}} \cdot r^{\alpha+1} \quad (1)$$

Examining $\Delta(\hat{Q})$, we see that the instability of the projection matrix is $O(B^{-0.5})$. When comparing DDP and local gradients: DDP's gradient has an effective batch size of MB ; the per-worker gradient with local batch size B is

aggregated across M workers. When using local gradients, however, the effective batch size is the local batch size. Determining projections locally yields a significantly noisier approximation than DDP. We also observe a dependence on the choice of rank r . In cases where $r \ll p, q$, there is less instability in the projection as it captures the most important dimensions of the signal, ignoring the noisy tail. As $r \rightarrow m, n$, the projection becomes more unstable due to noise affecting the basis estimation, providing a mathematical insight into the regularization induced by compression observed by [Robert et al. \(2025\)](#). Our results in Section 5.3 show that smaller batch sizes disproportionately impact local methods due to this noise sensitivity.

Global Projections as a Solution. Instead, we propose to use *global* projections that are shared across all workers at the synchronization boundary; this guarantees that all workers optimize within the same subspace. Specifically, Q_t is computed from the aggregated pseudo-gradient Δ_t , which represents the total change in model parameters following K local optimization steps. Furthermore, as in DDP, the pseudo-gradient has an effective batch size of MB , because it is aggregated across workers, yielding a more stable signal with reduced variance. We further posit that the pseudo-gradient is more informative as it contains curvature information baked into the pseudo-gradient signal, which is not available by purely observing the local gradient. We present a more detailed discussion of this in Section E.3.

3.2. Enabling Full Subspace Exploration

Although the global projection in Section 3.1 is theoretically superior, as it unifies worker optimization directions and leverages a higher-quality projection basis, it is guaranteed to restrict learning to a stagnant subspace. We propose that adding a full-rank quasi-hyperbolic momentum term alleviates this stagnation by injecting a full-rank signal into the pseudo-gradient, allowing full subspace exploration.

Stagnant Learning. Computing the aggregated pseudo-gradient after a K window of local training with low-rank optimization (derivations in Section B.3):

$$\Delta_t \leftarrow \underbrace{\frac{1}{|M|} \sum_{m=1}^M \sum_{\tau=t-K}^t \eta_\tau^m Q_\tau^m \alpha_\tau^m}_{\text{Local}} \quad \Delta_t \leftarrow \underbrace{\frac{1}{|M|} Q_t \sum_{m=1}^M \sum_{\tau=t-K}^t \eta_\tau^m \alpha_\tau^m}_{\text{Global}}$$

In this form, we observe LoRDO-Global effectively truncates the aggregated pseudo-gradient Δ_t to an r -rank subspace defined by the global projection matrix. Any optimization step on Δ_t is guaranteed to use a signal that is at most of rank r , reducing the possible optimization directions. Moreover, every new projection computed from this pseudo-gradient signal returns the same rank r subspace.

LoRDO-Local does not suffer from the same pathology: the summation of mutually orthogonal projection matrices recovers the full representation ([Horn & Johnson, 1985](#)). As such, both DDP and the *local* variant can fully explore the solution space.

Full-Rank Quasi-Hyperbolic Momenta. We posit that applying quasi-hyperbolic momentum terms to LoRDO-Global will bypass this aforementioned pathology by injecting a full-rank signal into the pseudo-gradient update, in addition to improving performance ([Iacob et al., 2026a](#)). In low-rank optimizers, quasi-hyperbolic momentum terms can be applied in one of two forms, where $\mu(z) = \frac{1}{r} \sum_{i=1}^r z_i$:

$$Q_t^m \left[\frac{(\omega u_t^m + (1 - \omega) \hat{g}_t^m)}{\sqrt{v_t^m} + \epsilon} \right] \text{ Low-Rank QHM}$$

$$(1 - \omega) \frac{\hat{G}_t^m}{\mu(\sqrt{v_t^m} + \epsilon)} + \omega Q_t^m \left[\frac{u_t^m}{\sqrt{v_t^m} + \epsilon} \right] \text{ Full-Rank QHM}$$

In its low-rank form, the quasi-hyperbolic moment is constrained to the same low-rank basis of the global projection matrix. However, by applying the gradient signal following the up-projection, scaled based on the second momentum, a full-rank signal is injected into the pseudo-gradient. This guarantees that the aggregated pseudo-gradient has full rank, enabling complete subspace exploration.

Additional Considerations. Following [Robert et al. \(2025\)](#), we always rotate momenta following the computation of a new projection matrix to ensure that momentum updates are always accumulated on the same subspace. Additionally, we use error-feedback locally, similar to [Robert et al. \(2025\)](#); [Seide et al. \(2014\)](#), to improve the performance of the local optimization procedure. We provide an ablation for both of these aspects in Figures 6 and 7, respectively. We discuss the limitations of our approach in Section A.

LoRDO Communication and Memory Savings. Compared to DDP with low-rank optimizers, using LoRDO realizes a communication benefit of $(\frac{1+\frac{r}{q}}{K_x} + \frac{1}{K_u} + \frac{1}{K_v})^{-1}$ due to its infrequent communication ([Iacob et al., 2026b](#)). In the case of DDP with full-rank Adam, this reduction improves to $(\frac{1+\frac{r}{q}}{K_x} + \frac{r}{K_u \cdot p} + \frac{r}{K_v \cdot p})^{-1}$ due to the low-rank optimizer states, in addition to the lower optimizer state memory overhead of $O(\frac{p}{r})$. For communication-efficient training methods using Adam locally, LoRDO-Global reduces communication and memory overhead by $\frac{3pq}{pq + pr + 2rq}$. Transmitting the global projection matrix to workers penalizes LoRDO-Global relative to LoRDO-Local. Yet, this overhead is negligible given $r \ll p, q$ in the regimes for which LoRDO is designed. We provide a more detailed discussion of these points in Sections B.5 and B.6.

4. Experimental Framework

Building on our theoretical motivations in Section 3, we investigate the following research questions:

- RQ1** Do global projections stagnate learning, as predicted?
- RQ2** Do full-rank quasi-hyperbolic momentum terms alleviate stagnation, as predicted?
- RQ3** Does LoRDO-Global benefit from a larger effective batch size, as per Section 3?
- RQ4** What is the dependence between the synchronization and rank?
- RQ5** How does LoRDO perform against DDP at scale?

4.1. Setup

Models and Data. Our experiments utilize peri-norm (Kim et al., 2025) decoder-only transformers scaled to 16M, 125M, and 720M parameters, as detailed in Table 4. The 16M variant is used for tuning various hyperparameters (see Section G) and qualitative analysis; the 125M and 720M variants are dedicated to investigating scaling behavior, and for baseline comparisons. We train all models on the SmolLM2 data mixture (Allal et al., 2025) using a sequence length of 2048. For further details, see Section D.

Optimizers and Tuning Methodology. Our methods are inspired by the GaLore and LDAdam (Zhao et al., 2024; Robert et al., 2025), initially designed as a low-rank counterpart to Adam (Kingma & Ba, 2015; Loshchilov & Hutter, 2019). Unless otherwise stated, all low-rank methods implement error-feedback (Seide et al., 2014) locally; see more details in Section E.1. For non-QHM experiments, we use $\beta_1 = 0.9$, $\beta_2 = 0.999$ as recommended by Semenov et al. (2025). For the QHM experiments, we independently tune the optimal ω 's and learning rates η for LoRDO-Global and LoRDO-Local, fixing $\beta_1 = 0.999$. Additionally, we leverage the CompleteP parametrization to transfer the optimal learning rate from the 16M model to our larger models. The DDP baselines independently tune their ω , η parameters. For more details, see Section G

Baselines. We compare LoRDO-Global and LoRDO-Local against: i) a DDP analogue using GaLore as the optimizer with LDAdam-style momenta rotations at various ranks, guaranteeing projection matrix update frequency is consistent across DDP and LoRDO, and ii) the full-rank counterparts using Adam for both the DDP setting and the communication-efficient setting. For all infrequent communication training methods, we use the stateful, and provably convergent, approaches of Local Adam (Cheng & Glasgow, 2025) for non-quasi-hyperbolic experiments, and MT-DAO for quasi-hyperbolic experiments, where we set $K = K_x = K_u = K_v = 32$ by default. This extends decoupled sync frequencies as Iacob et al. (2026b);

however, this is left for future work. We evaluate ML performance for communication-efficient methods under the same fixed synchronization frequency following prior work (Charles et al., 2025). We split the dataset in an IID fashion across 4 workers using $1 \times$ H100 per worker.

Metrics Our primary evaluation metric is the mean perplexity across workers. Additionally, we measure how similar the bases of two consecutive rotation matrices Q_t and Q_{t-1} using the Mean Squared Singular Value $MSSV = \frac{1}{r} \sum_{i=1}^r \sigma_i^2$ of the rotated basis matrix $R_t = Q_t^\top Q_{t-1}$. We also report the r^{th} spectral gap of a matrix U , which is the difference $\sigma_r - \sigma_{r+1}$ of the eigenvalues and we report the stable rank of a matrix U where $\text{sr}(U) = \|U\|_F^2 / \|U\|_2^2$.

5. Evaluation and Discussion

In this section, we provide a detailed evaluation of LoRDO, where we validate our theoretical findings, namely that i) global projections are superior only when full subspace exploration is enabled (Sections 5.1 to 5.3), ii) lower ranks are more sensitive to delayed communication (Section 5.4) and iii) that near-parity with DDP is reached at scale (Section 5.5). We defer all additional ablations to Section E.

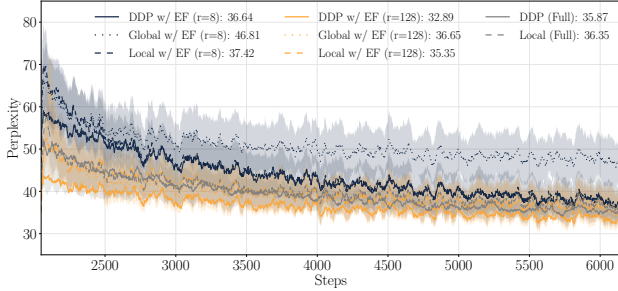
5.1. Naïve Global Projections Stagnate Learning (RQ1)

We begin our evaluation by analyzing whether a global projection matrix, without a full-rank quasi-hyperbolic momentum term, stagnates learning, as shown in Figure 1a. Validating our derivations in Section 3, ensuring a global projection is superior in the first few steps of training, following the warmup period, as it uses a projection matrix that is obtained from higher quality pseudo-gradients relative to the per-worker-generated projection matrix. However, the model fails to maintain this improvement as it is unable to update its r -rank subspace (Figure 1b), as predicted. LoRDO-Local, instead, explores the full solution space by refreshing its projection matrices throughout the duration of training (Figure 1b). Additionally, we see that LoRDO-Local maintains the same regularizing properties as seen in Robert et al. (2025), where methods of lower rank are able to match or outperform their high-rank variants.

Stagnated Subspace: Without full-rank signals, the LoRDO-Global stagnates learning; all workers optimize within a specific r -rank subspace determined by the first server's projection matrix for the duration of training.

5.2. LoRDO Enables Full Exploration (RQ2)

In Figure 2a, we show that injecting a full-rank quasi-hyperbolic momentum term alleviates learning stagnation, allowing for full subspace exploration. Across lower ranks ($r \in \{8, 16, 32, 64\}$), LoRDO-Global consistently out-



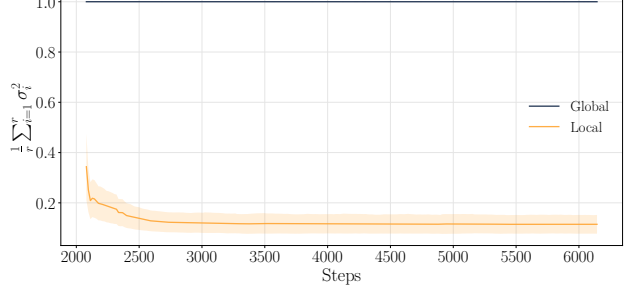
(a) Training curves for 16M models using the global and local projections, compared to the DDP baseline without quasi-hyperbolic momentum terms across "low-rank" ($r = 8$) and "high-rank" ($r = 128$) variants.

Figure 1. Global projection matrix pathologies. LoRDO-Global fails to learn when quasi-hyperbolic momentum terms have not been applied due to the projection bases failing to update throughout the duration of local training.

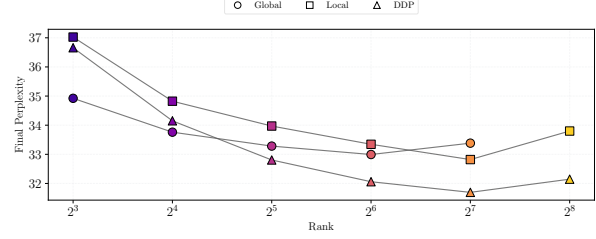
performs its local variant, and more readily matches the performance of the DDP counterpart, where LoRDO-Global and LoRDO-Local recover MT-DAO (Iacob et al., 2026a) when a full-rank representation is reached. To determine the cause of this performance result, we focus on the stable rank and the signal used to determine the projection, and the spectral gap of the resulting projection, in Figure 3.

Figure 3 shows that while the spectral gap of the two methods decreases as the projection rank increases, as is expected due to the power assumption (Xie et al., 2023), the spectral gap of the global projection, which leverages the aggregated pseudo-gradient, is orders of magnitude larger than the local counterpart. Observing full derivation of the matrix instability $\Delta(\hat{Q})$ in Section B.8, an increase in the stable rank is inversely proportional to the instability of the projection matrix $\Delta(\hat{Q}) \propto \frac{1}{\delta_r}$. This supports our derivations in Section 3, which show that using a local projection matrix is a suboptimal choice. Furthermore, unlike LoRDO-Local, whose stable rank remains consistent across projection ranks, the LoRDO-Global displays an inverse dependence across projection ranks. We argue that, since the pseudo-gradient has a richer history (including curvature information) for use in SVD, it is better able to identify principled directions that are more beneficial for the global optimization procedure. However, this comes at the cost of increased noise sensitivity as r increases, leading to greater instability. We provide a more detailed ablation in Section E.3.

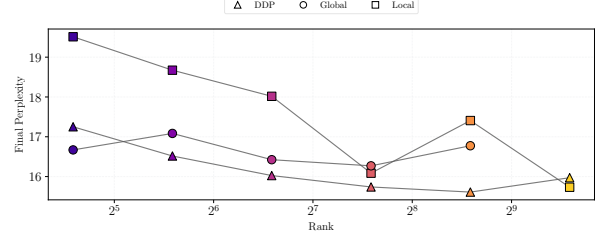
LoRDO Improves Stability and Performance: When applying a full-rank quasi-hyperbolic momentum, the LoRDO-Global is able to benefit from i) unifying the bases across workers and ii) providing a higher quality projection matrix. This results in an improved optimization trajectory relative to LoRDO-Local, especially at lower ranks.



(b) MSSV of the rotation matrix $R_t = Q_t^\top Q_{t-1}$ for the global and local projections. While the LoRDO-Local is able to effectively refresh its projection matrices and explore the full solution space, LoRDO-Global remains stagnant.



(a) Final perplexity for 125M models trained with LoRDO variants compared to DDP.



(b) Final perplexity for 125M models trained with LoRDO variants compared to DDP.

Figure 2. LoRDO with global projections offers superior resilience to small-batch regimes compared to the local projection method. Particularly under heavy memory constraints, which necessitate low ranks, LoRDO surpasses DDP.

5.3. LoRDO-Global Improves Projection Quality (RQ3)

In Figure 4, we present an ablation across the number of workers and the batch size used in our 16M parameter experiments to investigate whether the stability of the projection matrix depends on the effective batch size, as we identified in Section 3. Throughout, the global batch size $|B_G|$ is fixed to 64, and we alter the number of workers $|M|$ and the local batch size $|B|$. As predicted, LoRDO-Global is much less sensitive to changes in the number of workers

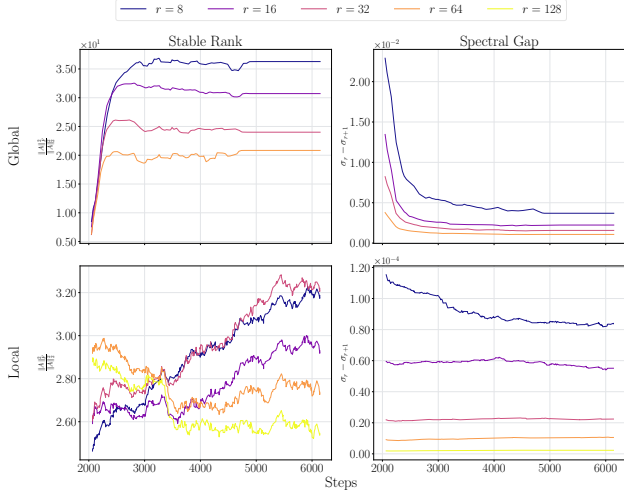


Figure 3. Stable rank (left column) and spectral gap (right column) for the attention layers on the 16M parameter model for LoRDO-Global (top row) and LoRDO-Local (bottom row) of LoRDO.

than the local variant, because its projection is based on the pseudo-gradient aggregate across workers, with a batch size of $|MB|$. Given that LoRDO-Local uses gradients with a batch size B , it quickly becomes destabilized as it enters a noise-dominated regime when B decreases.

Global Projections Improve Stability: Since the stability of the projection matrix scales with $O(\frac{1}{\sqrt{B}})$ (see Section 3), using the global pseudo-gradient improves the projection stability as the worker batch size decreases.

5.4. Lower Ranks Are Less Tolerant To More Infrequent Synchronization (RQ4)

We now investigate the interaction between the synchronization interval, where we fix $K_x = K_u = K_v = K$ for simplicity, and the rank chosen for LoRDO. In Figure 5, we present this ablation for a “low-” and “high-rank” setting of global and LoRDO-Local with/without the quasi-hyperbolic term. Irrespective of the quasi-hyperbolic term, we find that lower ranks ($r = 8$) are more sensitive to decreases in the synchronization frequency. Specifically, as the synchronization frequency is lowered (i.e., higher K), lower-rank variants are more likely to deviate from their high-synchronization counterparts and potentially diverge during training. In higher-rank regimes ($r = 128$), there is less difference across the synchronization frequencies. We also note that applying quasi-hyperbolic momentum terms reduces the extent to which this affects performance, although rank-level sensitivity persists. We posit this is due to the higher β_1 offering a longer half-life to the first momentum term, allowing it to be synchronized less often (see Jacob et al. (2026a)).

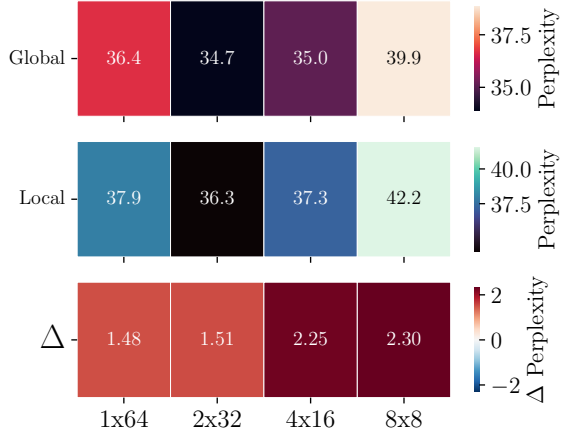


Figure 4. Ablation across number of workers and local batch size ($M \times B$) for 16M parameter experiments where the global batch size (or effective batch size) is 64. We present this ablation for both LoRDO-Global and Local and the difference $\Delta = PPX_{\text{Local}} - PPX_{\text{Global}}$. As predicted, we find that LoRDO-Local is more sensitive to changes in the local batch size.

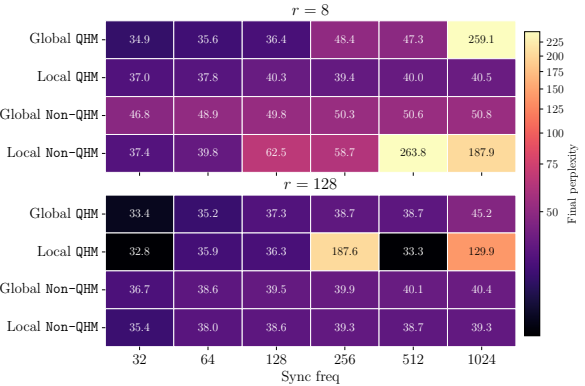


Figure 5. Ablation across synchronization frequency for LoRDO variants and QHM terms. Lower ranks are more sensitive to delays in synchronization. In addition to offering more stable performance, QHM terms reduce this sensitivity with an increased β_1 .

Low Ranks Are Sensitive to Sync Freq: Lower ranks are more sensitive to infrequent synchronization. Quasi-hyperbolic momentum mitigates this instability, maintaining performance while reducing communication overhead.

5.5. LoRDO Maintains Benefit at Scale (RQ5)

To determine LoRDO’s practical benefit at scale, we use it to train the 125M and 720M scales as seen in Figure 2b and Table 1, respectively. In the case of the 720M results, we select $r = 256$ such that this provides an $8 \times$ improvement for the optimizer state overhead relative to the full $r = 2048$ counterpart. We complement our perplexity results with a downstream task evaluation, reporting per-task and average task performance. We present results across the full training

duration for the 720M model in Figure 10.

Observing Figure 2b, LoRDO-Global maintains its superior performance over LoRDO-Local, where this is the most pronounced in lower rank regimes, as in the 16M case. Scaling to 720M parameters, we find that the benefit of LoRDO becomes effectively indistinguishable from its low-rank DDP counterpart. Specifically, LoRDO exhibits a reduction in perplexity of less than 1%, providing the same performance in downstream benchmarks, while achieving a communication reduction of 10 \times . LoRDO-Global maintains its benefits for communication-efficient training by reducing the communication overhead of full-rank DDP by $\approx 25\times$ and the memory overhead for the optimizer states by 8 \times . Additionally LoRDO-Global reduces the memory and communication overhead for optimizer states by 8 \times .

Table 1. 720M results comparison across final perplexity and downstream task accuracy. LoRDO matches its low-rank DDP counterparts, while substantially reducing communication.

Metric	r = 256			r = 2048	
	DDP	LoRDO-Local	LoRDO-Global	MT-DAO	DDP
ARC-Challenge (0-shot)	28.8	29.2	30.5	31.3	31.0
ARC-Easy (0-shot)	55.5	55.1	54.7	56.6	57.2
HellaSwag (0-shot)	40.3	40.0	40.1	42.2	43.2
MMLU (5-shot)	31.1	30.6	31.0	31.3	31.3
PIQA (0-shot)	68.6	68.6	67.1	68.3	69.2
Avg. All Tasks	44.8	44.7	44.7	45.9	46.4
Perplexity	10.34	10.56	10.41	9.98	9.85

LoRDO is Performant at Scale: LoRDO provides near-parity with its low-rank DDP counterpart across scales, in both perplexity and downstream task performance, showing that competitive performance can be achieved with significantly lower communication overhead. Furthermore, it remains competitive with the full-rank methods despite an 8 \times reduction in memory and communication costs.

6. Related Work

Distributed Training with Infrequent Communication. Prior research has focused on local update methods to mitigate the communication bottlenecks of standard Distributed Data Parallelism (DDP). Local SGD (Stich, 2019) enables workers to perform multiple local steps before averaging parameters. In LLM pre-training, DiLoCo (Charles et al., 2025) achieved high performance by combining local updates with Nesterov momentum as an outer optimizer. Local Adam (Cheng & Glasgow, 2025) proved convergence for adaptive optimizers by synchronizing all states, albeit tripling communication costs. DES-LOC (Jacob et al., 2026b) improved this by decoupling parameter and momenta synchronization. Our work builds on this mult-timescale framework, primarily targeting the memory constraints of full-rank optimizer states.

Optimization via Low-Rank Gradient Projection. Un-

like LoRA (Hu et al., 2022), which restricts optimization to adapters, GaLore (Zhao et al., 2024) projects full-rank gradients into a low-rank subspace via SVD, reducing memory without altering training dynamics. LDAdam (Robert et al., 2025) enhances this with Block Power Iteration and error feedback, while Dion (Ahn et al., 2025) uses rank- r orthogonalization to reduce overhead. These methods reduce memory in synchronous settings but have not been adapted for infrequent synchronization.

Distinction from Communication Compression Methods. A parallel line of work reduces communication volume via payload compression techniques such as quantization (Alistarh et al., 2017), sparsification (Lin et al., 2018), or mixes thereof, as seen in **CocktailSGD** (Wang et al., 2023), **DiLoCoX** (Qi et al., 2025), and **SparseLoCo** (Sarfi et al., 2025). We distinguish our approach from these methods on three critical grounds. First, these methods compress the pseudo-gradient only for transmission and do not reduce local memory costs. Second, they perform compression after local training, which can degrade model quality; conversely, optimization directly in a low-rank subspace has been shown to match or improve performance due to implicit regularization effects (Robert et al., 2025), a finding corroborated by our empirical results, while providing the communication benefits as a byproduct. Third, purely compression-based methods do not account for the transmission of optimizer states, which is known to be necessary for convergence guarantees and stability (Cheng & Glasgow, 2025). While our method does not inherently require state transmission, its intrinsic low-rank structure offers a principled compression mechanism. This reduces communication costs in proportion to the rank reduction, making the transmission of states more practical. Section F presents an extended overview.

7. Conclusion

LoRDO resolves the tension between projection stability and subspace exploration in low-rank communication-efficient optimization. By using an aggregated pseudo-gradient with full-rank quasi-hyperbolic momentum terms incorporated in the local update, we eliminate subspace stagnation without incurring the high variance of local methods. This principled design matches the performance of synchronous low-rank DDP at scale while communicating $\approx 25\times$ less. Furthermore, it reduces optimizer memory and communication costs by up to 12 \times compared to previous principled communication-efficient adaptive optimizers. Crucially, LoRDO exhibits superior resilience in memory-constrained settings, making pre-training feasible on hardware with limited resources. Ultimately, LoRDO extends model training beyond single data centers, paving the way for efficient learning in decentralized and memory and bandwidth-constrained environments.

Acknowledgements

This research was supported by the following entities: The Royal Academy of Engineering via DANTE (a RAEEng Chair); the European Research Council, specifically the REDIAL project; SPRIND under the composite learning challenge; Google through a Google Academic Research Award; in addition to the Ministry of Education of Romania (through the Credit and Scholarship Agency). MS was supported by Research England under the Expanding Excellence in England (E3) funding stream, which was awarded to MARS: Mathematics for AI in Real-world Systems in the School of Mathematical Sciences at Lancaster University.

Impact Statement

This paper presents work whose goal is to advance the field of machine learning. There are many potential societal consequences of our work, none of which we feel must be specifically highlighted here.

References

Ahn, K., Xu, B., Abreu, N., and Langford, J. Dion: Distributed orthonormalized updates. *arXiv preprint arXiv: 2504.05295*, 2025.

Alistarh, D., Grubic, D., Li, J., Tomioka, R., and Vojnovic, M. QSGD: communication-efficient SGD via gradient quantization and encoding. In *Conference on Neural Information Processing Systems (NeurIPS)*, 2017.

Allal, L. B., Lozhkov, A., Bakouch, E., Blázquez, G. M., Penedo, G., Tunstall, L., Marafioti, A., Kyd lícek, H., Lajarín, A. P., Srivastav, V., Lochner, J., Fahlgren, C., Nguyen, X., Fourrier, C., Burtenshaw, B., Larcher, H., Zhao, H., Zakka, C., Morlon, M., Raffel, C., and Wolf, T. Smollm2: When smol goes big - data-centric training of a small language model. *arXiv preprint arXiv:2502.02737*, 2025.

Bottou, L., Curtis, F. E., and Nocedal, J. Optimization methods for large-scale machine learning. *SIAM Review*, 2018.

Brown, T., Mann, B., Ryder, N., Subbiah, M., Kaplan, J. D., Dhariwal, P., Neelakantan, A., Shyam, P., Sastry, G., Askell, A., Agarwal, S., Herbert-Voss, A., Krueger, G., Henighan, T., Child, R., Ramesh, A., Ziegler, D., Wu, J., Winter, C., Hesse, C., Chen, M., Sigler, E., Litwin, M., Gray, S., Chess, B., Clark, J., Berner, C., McCandlish, S., Radford, A., Sutskever, I., and Amodei, D. Language models are few-shot learners. In *Conference on Neural Information Processing Systems (NeurIPS)*, 2020.

Charles, Z., Teston, G., Dery, L., Rush, K., Fallen, N., Garrett, Z., Szlam, A., and Douillard, A. Communication-efficient language model training scales reliably and robustly: Scaling laws for diloco. *arXiv preprint arXiv:2503.09799*, 2025.

Cheng, Z. and Glasgow, M. Convergence of distributed adaptive optimization with local updates. In *International Conference on Learning Representations (ICLR)*, 2025.

Davis, C. and Kahan, W. M. The rotation of eigenvectors by a perturbation. iii. *SIAM Journal on Numerical Analysis*, 1970.

DeepSeek-AI, Liu, A., Feng, B., Xue, B., Wang, B., Wu, B., Lu, C., Zhao, C., Deng, C., Zhang, C., Ruan, C., Dai, D., Guo, D., Yang, D., Chen, D., Ji, D., Li, E., Lin, F., Dai, F., Luo, F., Hao, G., Chen, G., Li, G., Zhang, H., Bao, H., Xu, H., Wang, H., Zhang, H., Ding, H., Xin, H., Gao, H., Li, H., Qu, H., Cai, J. L., Liang, J., Guo, J., Ni, J., Li, J., Wang, J., Chen, J., Chen, J., Yuan, J., Qiu, J., Li, J., Song, J., Dong, K., Hu, K., Gao, K., Guan, K., Huang, K., Yu, K., Wang, L., Zhang, L., Xu, L., Xia, L., Zhao, L., Wang, L., Zhang, L., Li, M., Wang, M., Zhang, M., Zhang, M., Tang, M., Li, M., Tian, N., Huang, P., Wang, P., Zhang, P., Wang, Q., Zhu, Q., Chen, Q., Du, Q., Chen, R. J., Jin, R. L., Ge, R., Zhang, R., Pan, R., Wang, R., Xu, R., Zhang, R., Chen, R., Li, S. S., Lu, S., Zhou, S., Chen, S., Wu, S., Ye, S., Ye, S., Ma, S., Wang, S., Zhou, S., Yu, S., Zhou, S., Pan, S., Wang, T., Yun, T., Pei, T., Sun, T., Xiao, W. L., Zeng, W., Zhao, W., An, W., Liu, W., Liang, W., Gao, W., Yu, W., Zhang, W., Li, X. Q., Jin, X., Wang, X., Bi, X., Liu, X., Wang, X., Shen, X., Chen, X., Zhang, X., Chen, X., Nie, X., Sun, X., Wang, X., Cheng, X., Liu, X., Xie, X., Liu, X., Yu, X., Song, X., Shan, X., Zhou, X., Yang, X., Li, X., Su, X., Lin, X., Li, Y. K., Wang, Y. Q., Wei, Y. X., Zhu, Y. X., Zhang, Y., Xu, Y., Xu, Y., Huang, Y., Li, Y., Zhao, Y., Sun, Y., Li, Y., Wang, Y., Yu, Y., Zheng, Y., Zhang, Y., Shi, Y., Xiong, Y., He, Y., Tang, Y., Piao, Y., Wang, Y., Tan, Y., Ma, Y., Liu, Y., Guo, Y., Wu, Y., Ou, Y., Zhu, Y., Wang, Y., Gong, Y., Zou, Y., He, Y., Zha, Y., Xiong, Y., Ma, Y., Yan, Y., Luo, Y., You, Y., Liu, Y., Zhou, Y., Wu, Z. F., Ren, Z. Z., Ren, Z., Sha, Z., Fu, Z., Xu, Z., Huang, Z., Zhang, Z., Xie, Z., Zhang, Z., Hao, Z., Gou, Z., Ma, Z., Yan, Z., Shao, Z., Xu, Z., Wu, Z., Zhang, Z., Li, Z., Gu, Z., Zhu, Z., Liu, Z., Li, Z., Xie, Z., Song, Z., Gao, Z., and Pan, Z. Deepseek-v3 technical report. *arXiv preprint arXiv:2412.19437*, 2025.

Dey, N., Zhang, B. C., Noci, L., Li, M. B., Bordelon, B., Bergsma, S., Pehlevan, C., Hanin, B., and Hestness, J. Don't be lazy: Completep enables compute-efficient deep transformers. *arXiv preprint arXiv: 2505.01618*, 2025.

Douillard, A., Feng, Q., Rusu, A. A., Chhaparia, R., Donchev, Y., Kuncoro, A., Ranzato, M., Szlam, A., and Shen, J. Diloco: Distributed low-communication training

of language models. *arXiv preprint arXiv:2311.08105*, 2023.

Douillard, A., Donchev, Y., Rush, K., Kale, S., Charles, Z., Garrett, Z., Teston, G., Lacey, D., McIlroy, R., Shen, J., Ramé, A., Szlam, A., Ranzato, M., and Barham, P. Streaming diloco with overlapping communication: Towards a distributed free lunch. *arXiv preprint arXiv:2501.18512*, 2025.

Dubey, A., Jauhri, A., Pandey, A., Kadian, A., Al-Dahle, A., Letman, A., Mathur, A., Schelten, A., Yang, A., Fan, A., Goyal, A., Hartshorn, A., Yang, A., Mitra, A., Srivankumar, A., Korenev, A., Hinsvark, A., Rao, A., Zhang, A., Rodriguez, A., Gregerson, A., Spataru, A., Rozière, B., Biron, B., Tang, B., Chern, B., Caucheteux, C., Nayak, C., Bi, C., Marra, C., McConnell, C., Keller, C., Touret, C., Wu, C., Wong, C., Ferrer, C. C., Nikolaidis, C., Al-lonsius, D., Song, D., Pintz, D., Livshits, D., Esiobu, D., Choudhary, D., Mahajan, D., Garcia-Olano, D., Perino, D., Hupkes, D., Lakomkin, E., AlBadawy, E., Lobanova, E., Dinan, E., Smith, E. M., Radenovic, F., Zhang, F., Synnaeve, G., Lee, G., Anderson, G. L., Nail, G., Mialon, G., Pang, G., Cucurell, G., Nguyen, H., Korevaar, H., Xu, H., Touvron, H., Zarov, I., Ibarra, I. A., Kloumann, I. M., Misra, I., Evtimov, I., Copet, J., Lee, J., Geffert, J., Vranes, J., Park, J., Mahadeokar, J., Shah, J., van der Linde, J., Billock, J., Hong, J., Lee, J., Fu, J., Chi, J., Huang, J., Liu, J., Wang, J., Yu, J., Bitton, J., Spisak, J., Park, J., Rocca, J., Johnstun, J., Saxe, J., Jia, J., Alwala, K. V., Upasani, K., Plawiak, K., Li, K., Heafield, K., Stone, K., and et al. The llama 3 herd of models. *arXiv preprint arXiv:2407.21783*, 2024.

Golub, G. H. and Reinsch, C. Singular value decomposition and least squares solutions. *Numerische Mathematik*, 14 (5):403–420, 1970.

Guastella, A., Sani, L., Iacob, A., Mora, A., Bellavista, P., and Lane, N. D. Sparsyfed: Sparse adaptive federated learning. In *International Conference on Learning Representations (ICLR)*, 2025.

Hägele, A., Bakouch, E., Kosson, A., Allal, L. B., von Werra, L., and Jaggi, M. Scaling laws and compute-optimal training beyond fixed training durations. In *Conference on Neural Information Processing Systems (NeurIPS)*, 2024.

Hoffmann, J., Borgeaud, S., Mensch, A., Buchatskaya, E., Cai, T., Rutherford, E., de Las Casas, D., Hendricks, L. A., Welbl, J., Clark, A., Hennigan, T., Noland, E., Millican, K., van den Driessche, G., Damoc, B., Guy, A., Osindero, S., Simonyan, K., Elsen, E., Rae, J. W., Vinyals, O., and Sifre, L. Training compute-optimal large language models. *arXiv preprint arXiv:2203.15556*, 2022.

Horn, R. A. and Johnson, C. R. *Matrix Analysis*. Cambridge University Press, 1985.

Hu, E. J., Shen, Y., Wallis, P., Allen-Zhu, Z., Li, Y., Wang, S., Wang, L., and Chen, W. Lora: Low-rank adaptation of large language models. In *The Tenth International Conference on Learning Representations, ICLR 2022, Virtual Event, April 25-29, 2022*. OpenReview.net, 2022.

Iacob, A., Jovanovic, A., Safaryan, M., Kurmanji, M., Sani, L., Horváth, S., Shen, W. F., Qiu, X., and Lane, N. D. MT-DAO: Multi-timescale distributed adaptive optimizers with local updates. In *International Conference on Learning Representations (ICLR)*, 2026a.

Iacob, A., Sani, L., Safaryan, M., Giampouras, P., Horváth, S., Jovanovic, A., Kurmanji, M., Aleksandrov, P., Shen, W. F., Qiu, X., and Lane, N. D. DES-LOC: Desynced low communication adaptive optimizers for foundation models. In *International Conference on Learning Representations (ICLR)*, 2026b.

Jordan, K., Jin, Y., Boza, V., You, J., Cesista, F., Newhouse, L., and Bernstein, J. Muon: An optimizer for hidden layers in neural networks, 2024. URL <https://kellerjordan.github.io/posts/muon/>.

Karimireddy, S. P., Jaggi, M., Kale, S., Mohri, M., Reddi, S. J., Stich, S. U., and Suresh, A. T. Mime: Mimicking centralized stochastic algorithms in federated learning. *arXiv preprint arXiv:2008.03606*, 2020.

Kim, J., Lee, B., Park, C., Oh, Y., Kim, B., Yoo, T., Shin, S., Han, D., Shin, J., and Yoo, K. M. Peri-In: Revisiting layer normalization in the transformer architecture. *arXiv preprint arXiv: 2502.02732*, 2025.

Kingma, D. P. and Ba, J. Adam: A method for stochastic optimization. In *International Conference on Learning Representations (ICLR)*, 2015.

Lin, Y., Han, S., Mao, H., Wang, Y., and Dally, B. Deep gradient compression: Reducing the communication bandwidth for distributed training. In *International Conference on Learning Representations (ICLR)*, 2018.

Loshchilov, I. and Hutter, F. Decoupled weight decay regularization. In *International Conference on Learning Representations (ICLR)*, 2019.

McCandlish, S., Kaplan, J., Amodei, D., and Team, O. D. An empirical model of large-batch training. *arXiv preprint arXiv:1812.06162*, 2018.

McMahan, B., Moore, E., Ramage, D., Hampson, S., and y Arcas, B. A. Communication-efficient learning of deep networks from decentralized data. In *International Conference on Artificial Intelligence and Statistics (AISTATS)*, 2017.

Modoranu, I.-V., Safaryan, M., Schultheis, E., Ryabinin, M., Chumachenko, A., and Alistarh, D. Fft-based dynamic subspace selection for low-rank adaptive optimization of large language models. *arXiv preprint arXiv:2505.17967*, 2025.

Pagliardini, M., Ablin, P., and Grangier, D. The adEMAMix optimizer: Better, faster, older. In *International Conference on Learning Representations (ICLR)*, 2025.

Peng, B., Quesnelle, J., and Kingma, D. P. Demo: Decoupled momentum optimization. *arXiv preprint arXiv:2411.19870*, 2024.

Qi, J., Zhu, W., Li, L., Wu, M., Wu, Y., He, W., Gao, X., Zeng, J., and Heinrich, M. Diloco: A low-communication large-scale training framework for decentralized cluster. *arXiv preprint arXiv:2506.21263*, 2025.

Reddi, S. J., Charles, Z., Zaheer, M., Garrett, Z., Rush, K., Konečný, J., Kumar, S., and McMahan, H. B. Adaptive federated optimization. In *International Conference on Learning Representations (ICLR)*, 2021.

Robert, T., Safaryan, M., Modoranu, I., and Alistarh, D. Ladam: Adaptive optimization from low-dimensional gradient statistics. In *International Conference on Learning Representations (ICLR)*, 2025.

Sarfi, A., Thérien, B., Lidin, J., and Belilovsky, E. Communication efficient LLM pre-training with sparseloco. *arXiv preprint arXiv:2508.15706*, 2025.

Seide, F., Fu, H., Droppo, J., Li, G., and Yu, D. 1-bit stochastic gradient descent and its application to data-parallel distributed training of speech dnns. In *Interspeech*, 2014.

Semenov, A., Pagliardini, M., and Jaggi, M. Benchmarking optimizers for large language model pretraining. *arXiv preprint arXiv: 2509.01440*, 2025.

Stewart, G. W. and Guang Sun, J. *Matrix Perturbation Theory*. Academic Press, 1990.

Stich, S. U. Local SGD converges fast and communicates little. In *International Conference on Learning Representations (ICLR)*, 2019.

Su, J., Ahmed, M. H. M., Lu, Y., Pan, S., Bo, W., and Liu, Y. Roformer: Enhanced transformer with rotary position embedding. *Neurocomputing*, 2024.

Thérien, B., Huang, X., Rish, I., and Belilovsky, E. Muloco: Muon is a practical inner optimizer for diloco. *arXiv preprint arXiv:2505.23725*, 2025.

Touvron, H., Martin, L., Stone, K., Albert, P., Almahairi, A., Babaei, Y., Bashlykov, N., Batra, S., Bhargava, P., Bhosale, S., Bikel, D., Blecher, L., Ferrer, C. C., Chen, M., Cucurull, G., Esiobu, D., Fernandes, J., Fu, J., Fu, W., Fuller, B., Gao, C., Goswami, V., Goyal, N., Hartshorn, A., Hosseini, S., Hou, R., Inan, H., Kardas, M., Kerkez, V., Khabsa, M., Kloumann, I., Korenev, A., Koura, P. S., Lachaux, M.-A., Lavril, T., Lee, J., Liskovich, D., Lu, Y., Mao, Y., Martinet, X., Mihaylov, T., Mishra, P., Molybog, I., Nie, Y., Poulton, A., Reizenstein, J., Rungta, R., Saladi, K., Schelten, A., Silva, R., Smith, E. M., Subramanian, R., Tan, X. E., Tang, B., Taylor, R., Williams, A., Kuan, J. X., Xu, P., Yan, Z., Zarov, I., Zhang, Y., Fan, A., Kambadur, M., Narang, S., Rodriguez, A., Stojnic, R., Edunov, S., and Scialom, T. Llama 2: Open foundation and fine-tuned chat models. *arXiv preprint arXiv:2307.09288*, 2023.

Vogels, T., Karimireddy, S. P., and Jaggi, M. Powersgd: Practical low-rank gradient compression for distributed optimization. In *Conference on Neural Information Processing Systems (NeurIPS)*, 2019.

Wang, J., Lu, Y., Yuan, B., Chen, B., Liang, P., De Sa, C., Re, C., and Zhang, C. Cocktailsd: Fine-tuning foundation models over 500mbps networks. In *International Conference on Machine Learning (ICML)*, 2023.

Xie, Z., Tang, Q.-Y., Sun, M., and Li, P. On the overlooked structure of stochastic gradients. In *Conference on Neural Information Processing Systems (NeurIPS)*, 2023.

Zhang, H., Morwani, D., Vyas, N., Wu, J., Zou, D., Ghai, U., Foster, D., and Kakade, S. M. How does critical batch size scale in pre-training? In *International Conference on Learning Representations (ICLR)*, 2025.

Zhao, J., Zhang, Z., Chen, B., Wang, Z., Anandkumar, A., and Tian, Y. GaLore: Memory-efficient LLM training by gradient low-rank projection. In *International Conference on Machine Learning (ICML)*, 2024.

Appendix

Table of Contents

A Limitations	13
B Extended Mathematical Derivations	13
B.1 Unrolled Low-Rank Updates Through Time	13
B.2 Aggregated Pseudo-gradient without Quasi-hyperbolic Momentum Terms	13
B.3 Discussions on Truncated Rank Representations	14
B.4 The Impact of Quasi-hyperbolic Momentum Terms on Learning and on Up-Link Communication	15
B.5 Addressing Communication	15
B.6 LoRDO Worker Memory Overhead	16
B.7 A Brief Discussion on the Choice of Signal for LoRDO-Global	17
B.8 Derivation of Projection Matrix Instability	17
C Additional Algorithms	19
D Experiment Details	20
D.1 Architecture Details and Parametrization	20
E Additional Experiments	20
E.1 Ablation on the Importance of Error Feedback	20
E.2 Ablation on the Importance of Well-Positioned Momenta	20
E.3 Ablation: DDP Gradient versus LoRDO-Global	21
E.4 Ablation: Impact on Sparse Communication	22
E.5 Full 720M Results	22
F Extended Related Work	23
G Hyperparameter Tuning and Warm-up Procedure	24
G.1 Findings: Ablation on Low- and Full-Rank QHM	24
G.2 Non-Quasi-Hyperbolic Sweeps	25
G.3 DDP Quasi-Hyperbolic Sweeps	26
G.4 LoRDO Quasi-Hyperbolic Sweeps	28

A. Limitations

First, our empirical validation at the 720M scale is limited, as computational constraints prevented an analysis of trends across varying ranks. However, we posit that the trends observed at the 16M and 125M scales will hold. Second, while we derive theoretical communication and memory gains for LORDO, we do not provide empirical results confirming these bounds. Third, although we hypothesize that LORDO-Local causes interference when aggregating pseudo-gradients in Non-IID settings, we lack empirical results to validate this claim.

B. Extended Mathematical Derivations

B.1. Unrolled Low-Rank Updates Through Time

Below, we provide a full mathematical derivation of the local optimization procedure for a worker m to support the arguments presented in Section 3. Initially, we consider the effect of local optimization without any quasi-hyperbolic momentum terms.

We follow the setting of DES-LOC (Jacob et al., 2026b) and Local Adam (Cheng & Glasgow, 2025) (both of which encompass the typical FedOpt (Reddi et al., 2021) setting). At first, we consider the setting where we set the number of local steps K to one. This gives the following local update computation when using a low-rank adaptive optimizer:

$$\theta_{t+1}^m \leftarrow \theta_t - \eta_t^m Q_t^m \alpha_t^m \quad (2)$$

where θ_t is the model received by the worker at the previous synchronization boundary. Computing the per-worker pseudo-gradients:

$$\Delta_t^m \leftarrow \theta_t - \theta_{t+1}^m \quad (3)$$

$$\Delta_t^m \leftarrow \theta_t - (\theta_t - \eta_t^m Q_t^m \alpha_t^m) \quad (4)$$

$$\Delta_t^m \leftarrow \eta_t^m Q_t^m \alpha_t^m \quad (5)$$

Now, we increase the number of local steps to some generic amount K to construct similar decompositions, albeit unrolled through time.

$$\Delta_t^m \leftarrow \theta_{t-K} - \theta_t^m \quad (6)$$

$$\Delta_t^m \leftarrow \theta_{t-K} - (\theta_{t-1}^m - \eta_{t-1}^m Q_{t-1}^m \alpha_{t-1}^m) \quad (7)$$

$$\Delta_t^m \leftarrow \theta_{t-K} - (\theta_{t-2}^m - \eta_{t-2}^m Q_{t-2}^m \alpha_{t-2}^m - \eta_{t-1}^m Q_{t-1}^m \alpha_{t-1}^m) \quad (8)$$

$$\Delta_t^m \leftarrow \theta_{t-K} - (\theta_{t-K} - \sum_{\tau=t-K}^t \eta_{\tau}^m Q_{\tau}^m \alpha_{\tau}^m) \quad (9)$$

$$\Delta_t^m \leftarrow \sum_{\tau=t-K}^t \eta_{\tau}^m Q_{\tau}^m \alpha_{\tau}^m \quad (10)$$

B.2. Aggregated Pseudo-gradient without Quasi-hyperbolic Momentum Terms

As before, we ignore the learning rate. However, in this case, we have assumed that the projection matrix gets updates at every step, causing a dependence on the time axis, namely:

$$\sum_{\tau=t-K}^t Q_{\tau}^m \alpha_{\tau}^m \neq \sum_{\tau=t-K}^t Q_{\tau}^m \sum_{\tau=t-K}^t \alpha_{\tau}^m \quad (11)$$

However, if we instead assume, for example, that Q^m remains fixed for the entire local training trajectory (as is configured with GaLore Zhao et al. (2024) for each worker in our experiments), or if each worker m receives a global projection matrix Q , we can derive the following update as the low rank projection matrix no longer depends on the local step:

$$\Delta_t^m \leftarrow Q^m \sum_{\tau=t-K}^t \eta_{\tau}^m \alpha_{\tau}^m \text{ or } \Delta_t^m \leftarrow Q \sum_{\tau=t-K}^t \eta_{\tau}^m \alpha_{\tau}^m \quad (12)$$

When viewed from the perspective of the global optimization step occurring on the outer optimizer:

$$\theta_{t+1} \leftarrow \theta_t - \eta_t^s \Delta_t \quad (13)$$

$$\theta_{t+1} \leftarrow \theta_t - \eta_t^s \frac{1}{|M|} \sum_{m=1}^M \Delta_t^m \quad (14)$$

$$\theta_{t+1} \leftarrow \theta_t - \eta_t^s \frac{1}{|M|} \sum_{m=1}^M \sum_{\tau=t-K}^t \eta_\tau^m Q_\tau^m \alpha_\tau^m \quad (15)$$

In the case of using a fixed local projection matrix, as is the case for LORDO-Local:

$$\theta_{t+1} \leftarrow \theta_t - \eta_t^s \underbrace{\frac{1}{|M|} \sum_{m=1}^M Q^m \sum_{\tau=t-K}^t \eta_\tau^m \alpha_\tau^m}_{\text{Pseudo-gradient signal}} \quad (16)$$

This modifies slightly in the case of ensuring a global projection matrix Q_t as is the case for LORDO-Global.

$$\theta_{t+1} \leftarrow \theta_t - \eta_t^s \underbrace{\frac{1}{|M|} Q_t \sum_{m=1}^M \sum_{\tau=t-K}^t \eta_\tau^m \alpha_\tau^m}_{\text{Pseudo-gradient signal}} \quad (17)$$

B.3. Discussions on Truncated Rank Representations

As discussed in Section 3, there are two solutions that emerge to determine the worker’s projection matrix: a *global* variant where each worker receives the same unified projection matrix, and a *local* variant where each worker determines its own projection matrix. While the global projections provide a more principled unification of the workers, and a higher quality projection matrix estimation, this introduces a subspace stagnation in the global optimization direction following the server accumulation without any full-rank quasi-hyperbolic momentum. Specifically, we present the aggregation step when accumulating the pseudo-gradient from M workers for the local (left, assuming the local projection matrix remains stagnant throughout the local training procedure) and global (right) variants (isolating the pseudo-gradient signal from Equations (16) and (17)):

$$\Delta_t \leftarrow \frac{1}{|M|} \sum_{m=1}^M \sum_{\tau=t-K}^t \eta_\tau^m Q_t^m \alpha_\tau^m \quad (18)$$

$$\Delta_t \leftarrow \frac{1}{|M|} \sum_{m=1}^M \sum_{\tau=t-K}^t \eta_\tau^m Q_t^m \alpha_\tau^m \quad (20)$$

$$\Delta_t \leftarrow \frac{1}{|M|} \sum_{m=1}^M Q^m \sum_{\tau=t-K}^t \eta_\tau^m \alpha_\tau^m \quad (19)$$

$$\Delta_t \leftarrow \frac{1}{|M|} Q \sum_{m=1}^M \sum_{\tau=t-K}^t \eta_\tau^m \alpha_\tau^m \quad (21)$$

In the case of the local model, as derived in Section B.1, we see that the projection matrix Q has no time dependence as we constrain it to remain constant for a window of K steps. However, each client has computed its own r -rank projection matrix, capturing the benefit of its local data distributions, enforcing the dependence across the worker aggregation. When aggregating the signal however, although we are summing across M $p \times q$ matrices that are of rank r , the overall pseudo-gradient signal Δ_t is a rank m matrix (we assume $m = n$ as is typical for the architectures we consider). The reason for this is that we are aggregating matrices that are potentially different (even orthogonal) subspaces of the original $p \times q$ space; the aggregation recovers a representation in the original space (Horn & Johnson, 1985).

The global projection, however, is independent across the time and worker axes as all workers share the same projection matrix Q . As such, when aggregating the signal, and then returning the projection to the full-rank basis, the pseudo-gradient signal is at best a rank r matrix; there was no diversity contributed from the individual data distributions available to each client. Consequently, when we compute the next projection matrix Q_{t+1} for LORDO-Global through an SVD operation,

the new projection lies entirely within the subspace spanned by the old projection matrix. The r bases of the previous projection matrix are indeed the top r most principled vectors of this new full dimensional space. As such, the projection matrix will never "refresh" at the synchronization interval. This does not happen in the local method as the workers each compute their own projection matrices on their local gradient signal. We visualize this pathology in Figure 1.

B.4. The Impact of Quasi-hyperbolic Momentum Terms on Learning and on Up-Link Communication

In Section 3.2, we introduced a novel contribution where we adapt quasi-hyperbolic momentum terms for low-rank optimizers. Specifically, we show that quasi-hyperbolic momentum terms can be introduced either in a low- or full-rank form. Below, we elucidate the impact this has on both the representation of low-rank optimization and the subsequent communication benefits that can be realized. We adapt the derivations to present the low- and full-rank quasi-hyperbolic momentum variants on the left and right, respectively, without making assumptions on the structure of the projection matrix.

$$\begin{aligned} \Delta_t &\leftarrow \frac{1}{|M|} \sum_{m=1}^K \sum_{\tau=t-K}^t \eta_\tau^m Q_t^m \alpha_\tau^m & \Delta_t &\leftarrow \frac{1}{|M|} \sum_{m=1}^M \sum_{\tau=t-K}^t \eta_\tau^m Q_t^m \alpha_\tau^m \\ \Delta_t &\leftarrow \frac{1}{|M|} \sum_{m=1}^K \sum_{\tau=t-K}^t \eta_\tau^m Q_t^m \left[\frac{\omega u_\tau^m + (1-\omega)\hat{g}_\tau^m}{\sqrt{v_\tau^m} + \epsilon} \right] & \Delta_t &\leftarrow \frac{1}{|M|} \sum_{m=1}^M \sum_{\tau=t-K}^t \eta_\tau^m \left((1-\omega) \frac{\hat{G}_\tau^m}{\mu(\sqrt{v_\tau^m} + \epsilon)} + \omega Q_t^m \left[\frac{u_\tau^m}{\sqrt{v_\tau^m} + \epsilon} \right] \right) \end{aligned}$$

Observing the structure of the low-rank quasi-hyperbolic momentum variant, we see that the additional signal is still constrained to the low-rank subspace determined by the projection matrix. In the case of LORDO-Global, adding the low-rank quasi-hyperbolic momentum term does not alleviate the stagnated learning pathology we observed in Section 3.

In the case of the full-rank quasi-hyperbolic term, we see that the signal becomes full-rank on each worker due to the injection of the full-rank gradient. As such, irrespective of whether one uses the local or global variant of LORDO, full subspace learning is guaranteed as the aggregated pseudo-gradient will always be full rank.

B.5. Addressing Communication

In this section, we provide a discussion into the communication overhead of LORDO. Table 2 summarises the per-payload communication amount across both DDP and the communication-efficient training regimes.

B.5.1. WORKER COMMUNICATION

Observing the above equations for local and LORDO-Global, we can realize an additional communication benefit on the model parameters (or pseudo-gradient). Instead of communicating the entire full-rank pseudo-gradient signal, we alleviate the communication overhead by decomposing the pseudo-gradient into its low-rank projection matrix and an accumulated update buffer across time. Notice that although the outer optimizer receives the two low-rank constructions, we are able to rebuild the full-rank pseudo-gradient signal as if this were rebuilt locally on each worker. In the case of a globally unified projection matrix, the communication cost reduces to just the accumulated low-rank pseudogradient through time as the server already stores a copy of the global projection matrix it sent to each worker. This derivation holds for all server-side aggregation strategies, not just averaging as we have used for the purposes of our experiments.

In the case of applying quasi-hyperbolic momentum terms, the same communication benefit can be realized should the quasi-hyperbolic momentum terms be applied in their low-rank form. However, if they are applied in the full-rank form, one can no longer decompose the pseudo-gradient signal. As such, the communication cost of this regime reverts to the same as communicating dense pseudo-gradients in the case of previous methods (Jacob et al., 2026a,b).

However, in these methods, not only are the parameters (or pseudo-gradients) communicated, but a similar operation is performed to synchronize the optimizer states which ensures provable convergence. In this regard, LORDO, which applies low-rank optimizers locally with a global projection matrix, also affords communication reduction as this rq low-rank structure is communicated instead of the pq matrix for each optimizer state.

B.5.2. ADDRESSING DOWN-LINK COMMUNICATION

Observing the construction presented in Equation (16), downlink communication for the local method is always guaranteed to be full rank. Given that each worker's projection matrix Q^m is non-identical, this element cannot be pulled out of the second summation, which would allow us to communicate two low rank structures as we did with the up-link communication. In

the case of the global variant, in the case of no global quasi-hyperbolic momentum, a reduction in down-link communication can be achieved. Assuming that each worker maintains the previous projection matrix Q_t and previously received model θ_t , each worker only needs to receive the aggregated low rank pseudo-gradient signal $\sum_{m=1}^M \sum_{\tau=t-K}^t \eta_\tau^m \alpha_\tau^m$ to compute the new model θ_{t+1} locally. In addition to this, each worker needs to receive the new globally computed projection matrix Q_{t+1} . In the case of LoRDO-Global with full-rank quasi-hyperbolic momentum terms, the pseudo-gradient update signal is indeed full rank, and thus no additional communication benefit can be achieved. Instead, LoRDO-Global incurs an additional $O(pr)$ cost to transmit the projection bases to each worker. However, given the fact that $r \ll p, q$, this additional communication cost is negligible, and is counteracted by the additional overhead afforded by synchronizing the momenta states in their low-rank forms.

Table 2. Communication Cost Comparison on a per-payload basis between DDP and LoRDO-Global/LoRDO-Local. We assume that the pseudo-gradient and momenta parameters are communicated at the same interval K

Method	QHM	Up-Link	Down-Link
Global	N/A	$O(3rq)$	$O(pr + 3rq)$
	Low	$O(3rq)$	$O(pr + 3rq)$
	Full	$O(pq + 2rq)$	$O(pq + pr + 2rq)$
Local w/ (Fixed Projection)	N/A	$O(pr + 3rq)$	$O(pq + 2rq)$
	Low	$O(pr + 3rq)$	$O(pq + 2rq)$
	Full	$O(pq + 2rq)$	$O(pq + 2rq)$
MT-DAO/ DES-LOC	–	$O(3pq)$	$O(3pq)$
DDP	–	$O(pq)$	$O(pq)$

B.5.3. UNDERSTANDING THE ROLE OF COMMUNICATION FREQUENCY

The primary communication benefit of training methods that employ local updates is that they reduce the communication frequency relative to DDP. As per [Jacob et al. \(2026b\)](#), the amount these regimes benefit from infrequent communication can be quantified by the following ratio:

$$\left(\frac{1}{K_x} + \frac{1}{K_u} + \frac{1}{K_v} \right)^{-1} \quad (22)$$

$$(23)$$

where K_x, K_u and K_v are the update frequencies of the model parameters and optimizer states respectively. Relative to a DDP optimizer using full-rank momenta (like Adam), we first realize a $\frac{p}{r} \times$ reduction in the memory overhead to transmit the low-rank momenta terms. This leads to an improvement of:

$$\left(\frac{1}{K_x} + \frac{1}{K_u \cdot (\frac{p}{r})} + \frac{1}{K_v \cdot (\frac{p}{r})} \right)^{-1} \quad (24)$$

in the case of LoRDO-Local where projection matrices are not determined globally. In the case of the latter, we incur a slight cost relative to DDP. Instead of transmitting only a dense pseudo-gradient (or model parameter) pq , we also transmit the global projection matrix of size pr to the workers. This changes the benefit of the LoRDO-Global regime to:

$$\left(\frac{1 + \frac{r}{q}}{K_x} + \frac{1}{K_u \cdot (\frac{p}{r})} + \frac{1}{K_v \cdot (\frac{p}{r})} \right)^{-1} \quad (25)$$

In any case, given that $r \ll p, q$, the additional overhead is negligible. When compared to communication-efficient regimes that use full-rank optimizers, the total benefit is $\frac{3pq}{pq+2rq}$ in the case of LoRDO-Local and $\frac{3pq}{pq+pr+2rq}$ in the case of LoRDO-Global.

B.6. LoRDO Worker Memory Overhead

In Table 3, we present the memory overhead complexity for each of the variants of LoRDO, relative to the full-rank Adam baseline. Across all variants, we see that the consistent trade-off in memory overhead is modulated by the choice of the rank

Table 3. Memory overhead for all LoRDO variants compared to full-rank counterparts.

	Gradient	Optimizer States	Projection Matrix	Uplink Time Buffer	Error Buffer	Overhead
Adam	$O(pq)$	$O(2pq)$	/	/	/	$O(3pq)$
LoRDO Global / Local No QHM	$O(rq)$	$O(2rq)$	$O(pr)$	/	$O(pq)$	$O(pq + pr + 3rq)$
LoRDO Global / Local Low-Rank QHM	$O(rq)$	$O(2rq)$	$O(pr)$	/	$O(pq)$	$O(pq + pr + 3rq)$
LoRDO Global / Local Full-Rank QHM	$O(pq + rq)$	$O(2rq)$	$O(pr)$	/	$O(pq)$	$O(pq + pr + 3rq)$
LoRDO Global / Local No QHM	$O(rq)$	$O(2rq)$	$O(pr)$	$O(rq)$	$O(pq)$	$O(pq + pr + 4rq)$
LoRDO Global / Local Low-Rank QHM	$O(rq)$	$O(2rq)$	$O(pr)$	$O(rq)$	$O(pq)$	$O(pq + pr + 4rq)$
LoRDO Global / Local Full-Rank QHM	$O(pq + rq)$	$O(2rq)$	$O(pr)$	/	$O(pq)$	$O(pq + pr + 3rq)$

r , as expected. Specifically, in cases where $r \ll p, q$, we observe significant memory savings as storing two matrices of pr and rq are considerably less intensive than a pq matrix.

An important characteristic of the communication savings of LoRDO can be observed in Table 3. Specifically, in order to realize the up-link cost savings in Section B.5.1, for the non- and low-rank quasihyperbolic momentum variants, each worker m incurs an additional $O(rq)$ cost to store the accumulated buffer across time between parameter synchronization periods. For full-rank methods, this structure is not possible; as such, it achieves a lower memory overhead traded for an increase in the communication payload size.

Finally, each worker incurs memory overhead to maintain the error-feedback buffer, which is the size of the full-rank gradient. However, as done by [Robert et al. \(2025\)](#), this error feedback buffer can be stored on the full-rank gradient variable for a memory-efficient implementation. This prevents LoRDO from being compatible with gradient accumulation techniques. However, this design space is opened to the practitioner to choose the optimal configuration given their hardware resources.

B.7. A Brief Discussion on the Choice of Signal for LoRDO-Global

In Section 3, we make the design decision to use the projection matrix to compute the global projection matrix Q_t . However, in distributed optimization, we also have the opportunity to use the optimizer states as well as the pseudo-gradient signal for this compression operation as they both materialize at the synchronization boundary. However, using the momenta terms instead of, or in concert with, the pseudo-gradient offers no benefit. By definition, the optimizer states are confined to the same subspace as the pseudo-gradient. Furthermore, if you perform SVD on the up-projected momentum signal, the optimal projection matrix that will be computed will be the same that was used in the previous iteration, as we showed in Section B.3.

B.8. Derivation of Projection Matrix Instability

Below, we provide a more rigorous derivation of the instability formula we had used in Section 3, where we repeat some of the definitions for convenience.

Assume that the stochastic gradient \hat{G} is a perturbed version of the true gradient G such that $\hat{G} = G + E$, where E represents the additive noise incurred through the stochastic sample. Furthermore, we assume that the noise scales proportional to $\frac{\kappa}{\sqrt{B}}$, where B is the batch size and κ is the variance of the individual samples ([McCandlish et al., 2018](#); [Bottou et al., 2018](#)). Additionally, as shown by [Xie et al. \(2023\)](#), we assume that the singular values of G and \hat{G} follow a power-law where $\sigma_k = Ck^{-\alpha}$ where $\alpha > 0$.

Using the Davis-Kahan sin Θ theorem ([Stewart & Guang Sun, 1990](#); [Davis & Kahan, 1970](#)), we quantify the stability of the

true r rank subspace Q and estimated subspace derived from \hat{G} :

$$\|\sin \Theta(Q, \hat{Q})\|_F \leq \frac{\|E\|_F}{\delta_r}$$

where δ_r represents the spectral gap ($\sigma_r - \sigma_{r+1}$). We quantify the instability of the projection matrix \hat{Q} as:

$$\Delta(\hat{Q}) \approx \frac{\|E\|_F}{\delta_r}$$

To approximate the spectral gap $\delta_r = \sigma_r - \sigma_{r+1}$, we treat the singular values as a continuous function of the rank index r . Given the power-law assumption $\sigma(k) = Ck^{-\alpha}$, the difference between two consecutive singular values corresponds to the magnitude of the gradient of the singular value curve at rank r . By applying the first-order Taylor approximation, we write:

$$\delta_r \approx \left| \frac{d\sigma(k)}{dk} \Big|_{k=r} \right|$$

Differentiating the power-law function with respect to k yields:

$$\frac{d}{dk} (Ck^{-\alpha}) = -\alpha C k^{-(\alpha+1)}$$

Taking the absolute value, we obtain the spectral gap approximation $\delta_r \approx \alpha C r^{-(\alpha+1)}$. Substituting this result and the noise estimate $\|E\|_F \approx \frac{\kappa}{\sqrt{B}}$ back into the instability inequality gives rise to:

$$\Delta(\hat{Q}) \approx \frac{\kappa/\sqrt{B}}{\alpha C r^{-(\alpha+1)}} = \frac{\kappa}{\alpha C \sqrt{B}} \cdot r^{\alpha+1}$$

C. Additional Algorithms

Algorithm 2 LORDO Local Variant - Bias Correction Omitted for Ease of Notation

Require: Model tensors, hyper-parameters

- 1: $T, M \in \mathbb{N}_+$ — total optimization steps and number of workers
- 2: $\beta_1, \beta_2 \in [0, 1], \omega \in [0, 1]$ — decay rates for each momentum state and QHM convex combination coefficients
- 3: $\rho \in \mathbb{R}_+, \{\eta_t\}_{t=0}^{T-1}$ — clipping radius, learning-rate schedule
- 4: $K_x, K_u, K_v \in \mathbb{N}_+$ — communication periods for parameters and states
- 5: $\text{OuterOpt} : (\mathbb{R}^d, \mathbb{R}^d) \rightarrow \mathbb{R}^d$ — update params using an outer optimizer, averaging by default
- 6: $\text{ComputeProjection} : (\mathbb{R}^{d \times d}, \mathbb{R}) \rightarrow \mathbb{R}^{d \times r}$ — Compute projection routine
- 7: $x_0^m = x_0 \in \mathbb{R}^d, u_{-1}^m = \mathbf{0}_r, v_{-1}^m = \mathbf{0}_r$ — initial params, first and second momentum
- 8: $Q_0 = \mathbb{I}^{d \times r}, E_{-1}^m = \mathbf{0}_{d \times d}, \forall m \in M$ - Identity initial projection matrix and zeroed-out error buffer for each client

Ensure: x_T, u_{T-1}, v_{T-1}

9: **for** $t = 0, \dots, T - 1$ **do**

```

10: for all workers  $m = 0, \dots, M - 1$  in parallel do
11:    $\hat{G}_t^m \leftarrow \text{clip}(\nabla F(x_t^m; \xi_t^m), \rho)$  Clipped stochastic gradient in full-rank
12:   if  $((t - 1) \bmod K_x = 0)$  then
13:      $Q_t^m \leftarrow \text{ComputeProjection}(\hat{G}_t^m + E_{t-1}^m)$  Update  $Q_t^m$  following  $K_x$  sync.
14:      $\bar{u}_{t-1}^m \leftarrow Q_t^m \top Q_{t-1}^m \bar{u}_{t-1}^m$  Compute a new global projection matrix with error feedback
15:      $\bar{v}_{t-1}^m \leftarrow (1 - \beta_2^m) \left| (Q_t^m \top Q_{t-1}^m)^2 (\hat{v}_{t-1}^m - (\hat{u}_{t-1}^m)^2) + (Q_t^m \top Q_{t-1}^m \hat{u}_{t-1}^m)^2 \right|$  Rotate the first moment locally
16:   else
17:      $Q_t^m = Q_{t-1}^m$  Rotate the second moment locally Maintain stale projection
18:      $\hat{g}_t^m \leftarrow Q_t^m \top (\hat{G}_t^m + E_{t-1}^m)$  Low-rank gradient signal with error-feedback
19:      $E_m^t \leftarrow \hat{G}_t^m + E_{t-1}^m - Q_t^m \hat{g}_t^m$  Compute error feedback
20:      $u_t^m \leftarrow \beta_1 \bar{u}_{t-1}^m + (1 - \beta_1) \hat{g}_t^m$ 
21:      $v_t^m \leftarrow \beta_2 \bar{v}_{t-1}^m + (1 - \beta_2) (\hat{g}_t^m)^2$ 
22:     
$$\bar{x}_t^m \leftarrow x_t^m - \eta_t \begin{cases} Q_t^m \left[ \frac{u_t^m}{\sqrt{v_t^m + \epsilon}} \right] & \text{No QHM} \\ Q_t^m \left[ \frac{\omega u_t^m + (1 - \omega) \hat{g}_t^m}{\sqrt{v_t^m + \epsilon}} \right] & \text{Low-Rank QHM} \\ (1 - \omega) \frac{\hat{G}_t^m}{\mu(\sqrt{v_t^m + \epsilon})} + \omega Q_t^m \left[ \frac{u_t^m}{\sqrt{v_t^m + \epsilon}} \right] & \text{Full-Rank QHM} \end{cases}$$

23:      $\bar{u}_t \leftarrow \text{if } (t \bmod K_u = 0) \text{ then } \mathbb{E}_m[u_t^m] \text{ else } u_t^m$  Sync  $u^j$  every  $K_u$ 
24:      $\bar{v}_t \leftarrow \text{if } (t \bmod K_v = 0) \text{ then } \mathbb{E}_m[v_t^m] \text{ else } v_t^m$  Sync  $v$  every  $K_v$ 
25:      $\Delta_t^m \leftarrow \bar{x}_t^m - x_{t-K_x}^m; \Delta_t \leftarrow \mathbb{E}_m[\Delta_t^m]$  Compute per-worker and aggregated pseudo-gradient
26:      $x_{t+1}^m \leftarrow \text{if } (t \bmod K_x = 0) \text{ then } \text{OuterOpt}(\Delta_t, x_{t-K_x}^m) \text{ else } \bar{x}_t^m$  Sync  $x$  every  $K_x$ 

```

D. Experiment Details

This section details the experimental framework, covering: model architecture and parametrization (Section D.1); the hyperparameter sweep procedure (Section G.2); and the tuning results for LORDO.

D.1. Architecture Details and Parametrization

Table 4. Model architecture and training hyperparameters used across experiments. We specify the number of (Blocks), attention heads (Heads), embedding dimension (d_{model}), vocabulary size ($|\mathcal{V}|$), and feedforward expansion ratio (Exp. Ratio) for each of the model sizes used in our experiments. Additionally, we show the global batch sizes ($|\mathcal{B}_G|$) and the total number of training steps (T) used in our experiments. Our models make use of RoPE positional embeddings (Su et al., 2024), SiLU as the activation function. Additionally, we adopt norm-based gradient clipping with a bound of ρ , which are initialized with a typical $\sigma = 0.02$, following guidance from Semenov et al. (2025); Dey et al. (2025). For our optimizers, we use the ρ values recommended by Semenov et al. (2025) for the relevant model scale. Additionally, we set a sequence length that is standard for models at these scales.

Model Size	Blocks	d_{model}	$ \mathcal{V} $	#Heads	Exp.~Ratio	RoPE θ	ACT	Init σ	ρ	Seq Len	$ \mathcal{B}_G $	T
16M	4	256	50K	4	4	10000	SiLU	0.02	1.0	2048	64	4608
125M	12	768	50K	12	4	10000	SiLU	0.02	0.5	2048	256	4608
720M	12	2048	50K	16	4	10000	SiLU	0.02	0.1	2048	512	10240

Table 4 summarizes the architectural specifications, which follow standard conventions for large language models of these sizes. To improve training stability and performance, we implement two key architectural modifications. First, we adopt the peri-LayerNorm design (Kim et al., 2025) instead of the standard pre-norm formulation. Second, we use the CompleteP parametrization (Dey et al., 2025) with $\alpha = 1.0$. This configuration enables one-shot hyperparameter transfer from small to large models, allowing us to conduct extensive sweeps on the 16M variant and reserve compute-intensive scaling experiments for baseline comparisons.

Batch sizes and training durations follow contemporary best practices (Zhang et al., 2025). For the 125M and 720M models, we adopt global batch sizes of 256 and 512, respectively, following Semenov et al. (2025); for the 16M model, we use a batch size of 64. Training steps T are set as multiples of the compute-optimal token budget (Hoffmann et al., 2022): the 16M model is trained for $\approx 2 \times$ the compute-optimal duration, while the 125M and 720M models are trained for $\approx 2 \times$ and $\approx 1 \times$ their respective budgets. All models utilize the Warmup-Stable-Decay (WSD) scheduler (Hägle et al., 2024). Warmup lengths follow recommendations from Zhang et al. (2025); Hägle et al. (2024); Allal et al. (2025); Semenov et al. (2025), with a fixed warmup period of $T_{\text{WARM}} = 2048$ steps across all experiments.

E. Additional Experiments

E.1. Ablation on the Importance of Error Feedback

As discussed in Section 3, in addition to our novel algorithmic improvements, we leverage error-feedback mechanisms (Seide et al., 2014) during the local optimization procedures for each worker to account for information lost during low-rank compression.

In Figure 6, we conduct an ablation on using error feedback across ranks and method types for our 16M model scales. Across all settings, we find error feedback is essential to ensuring good performance, consistent with Seide et al. (2014); Robert et al. (2025).

E.2. Ablation on the Importance of Well-Positioned Momenta

As mentioned in Section 3, we leverage the insight from Robert et al. (2025), who show that optimizer state rotation is essential once a new projection matrix is determined. We illustrate an ablation across this momenta rotation in our method in Figure 7 for our 16M models for both LORDO-Global and LORDO-Local with quasi-hyperbolic momentum terms applied. For both local and global methods, we find that rotating the momenta is essential for performance, corroborating the findings of Robert et al. (2025).

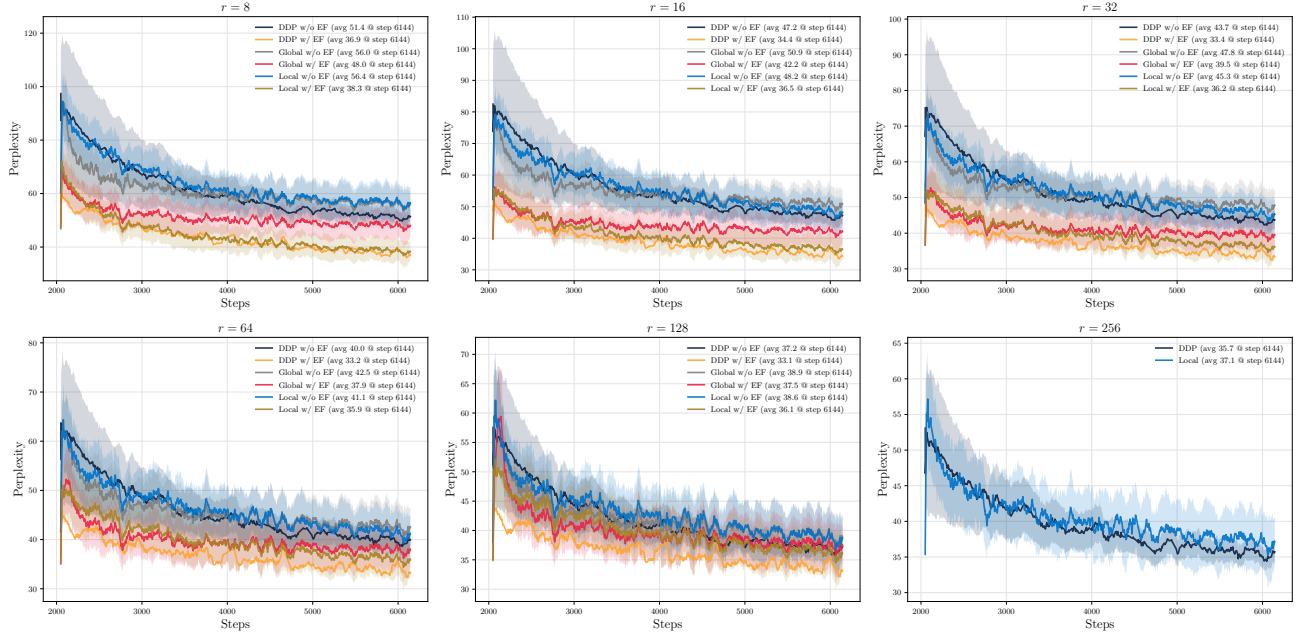


Figure 6. Impact of error feedback used during local optimization for DDP and the *global* and *local* variants of LoRDO across $r \in \{8, 16, 32, 64, 128, 256\}$, where $r = 256$ is the full-rank Adam baseline. Across all ranks and model classes, error feedback is essential for optimal performance, corroborating the findings of Seide et al. (2014); Robert et al. (2025).

E.3. Ablation: DDP Gradient versus LoRDO-Global

In Section 5, we observe that, particularly at lower ranks, LoRDO-Global significantly outperforms its DDP variant. We posit two factors causing these differences:

- i Allowing a larger exploration of the loss landscape (i.e., having a greater history due to the K step window) provides a more informative signal than the gradient.
- ii Integrating curvature information into the projection matrix computation creates more informative bases.

In Figure 8, we visualize the first component of this investigation, plotting both LoRDO-Global and LoRDO-Local across synchronization intervals $K \in \{1, 2, 4, 8, 16\}$. In the case of LoRDO-Local, we find effectively no difference when increasing the frequency at which subspaces are computed; the gradient signal remains consistently informative along this axis. However, with LoRDO-Global, performance improves as synchronization is delayed. We posit that this process allows each worker to explore a larger region of its loss landscape. Consequently, upon aggregation, this creates a signal

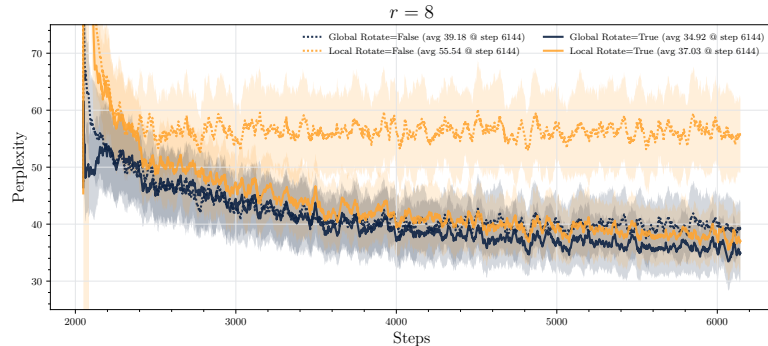


Figure 7. Importance of ensuring well-positioned momenta. Both local and global variants of LoRDO fail to learn effectively when optimizer states are not rotated into the new basis.

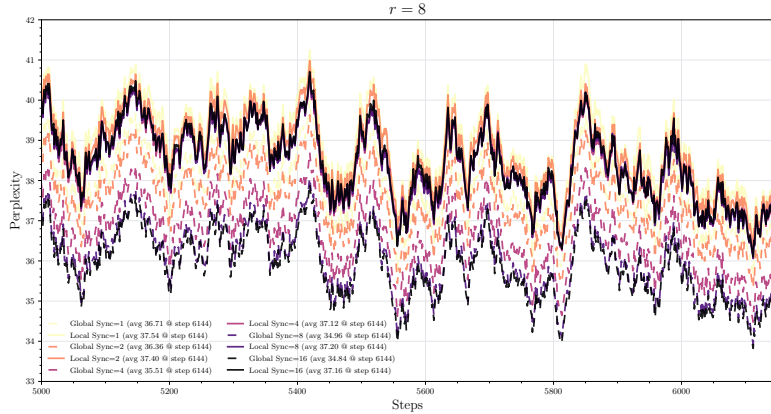


Figure 8. Ablation across increasing the synchronization frequency, and thus the frequency of projection matrix updates. We find that the performance of LORDO-Local remains relatively consistent across this axis, while LORDO-Global’s performance displays a dependence. This indicates that increasing the number of local steps (effectively increasing the history baked into the pseudo-gradient) is beneficial for determining optimal projection matrices for LORDO-Global.

that is more informative for the projection computation, as it possesses a greater history of information for determining the optimal basis.

For the second component, we examine the results of Figures 2a and 4. In Figure 4, although LORDO-Global uses a single worker to determine its projection matrix (after 32 steps of local training), its final perplexity is indistinguishable from its DDP counterpart in Figure 2a. This suggests that the curvature information baked into the pseudo-gradients of each worker helps determine a more informative projection matrix, especially considering LORDO’s performance improvement as the number of workers increases in Figure 4. We leave a thorough investigation on the interplay between projecting gradients and pseudo-gradients to future work.

E.4. Ablation: Impact on Sparse Communication

Although methods implementing communication compression at synchronization intervals are orthogonal to our work, we consider the effect of sparsification to additionally improve the communication overhead for LORDO. In Figure 9, we ablate across percentages of Top-K sparsity for both the global and local variants. As expected, we find that with increased sparsification, the performance of LORDO degrades regardless of whether projection matrices are determined locally or globally. There is less meaningful signal for the outer optimizer to learn a representation beneficial for the global optimization trajectory. Interestingly, we find that LORDO-Global is not more affected by sparsity than its local counterpart. We posit two reasons for this behavior. First, even though individual pseudo-gradients are sparse, their aggregation creates an informative signal—not necessarily sparse (Guastella et al., 2025)—that preserves the dominant directions necessary to determine a robust global projection matrix. Second, unlike the local variant, the LORDO-Global method employs full-rank quasi-hyperbolic momentum terms. This injects a full-rank signal into the update, allowing the optimizer to correct for meaningful directions potentially lost during the sparsification of the projection subspace. We leave a full investigation into the combination of communication compression and LORDO for future work.

E.5. Full 720M Results

In Section 5, we present the results for the 720M scale at the end of training for brevity. In Figure 10, we present the full set of results across the entire duration of training:

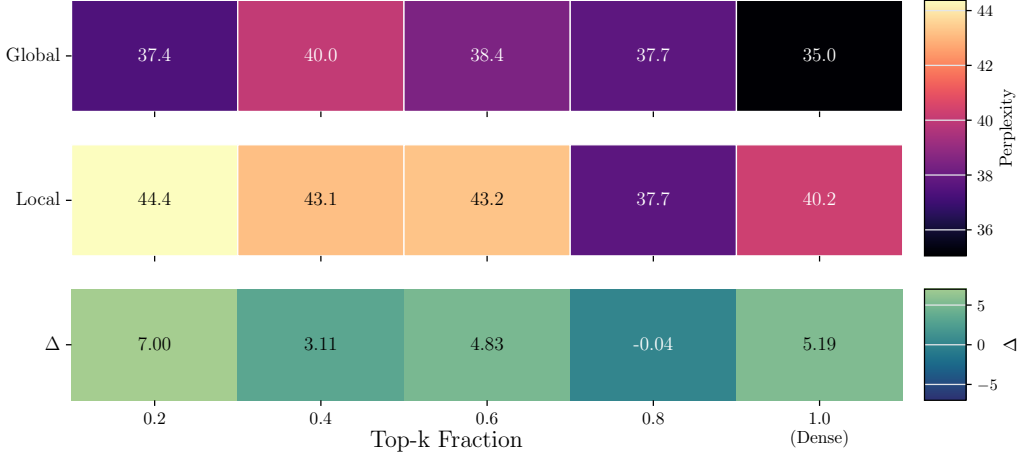


Figure 9. Ablation across sparsity levels for LORDO-Global and Local, reporting the final perplexity for each, along with the difference $\Delta = PPX_{\text{Local}} - PPX_{\text{Global}}$. We observe that while both methods are affected by increasing sparsity, the addition of the full-rank quasi-hyperbolic momentum signal allows for improved performance relative to LORDO-Local, despite using a potentially damaged projection matrix due to pseudo-gradient sparsification.

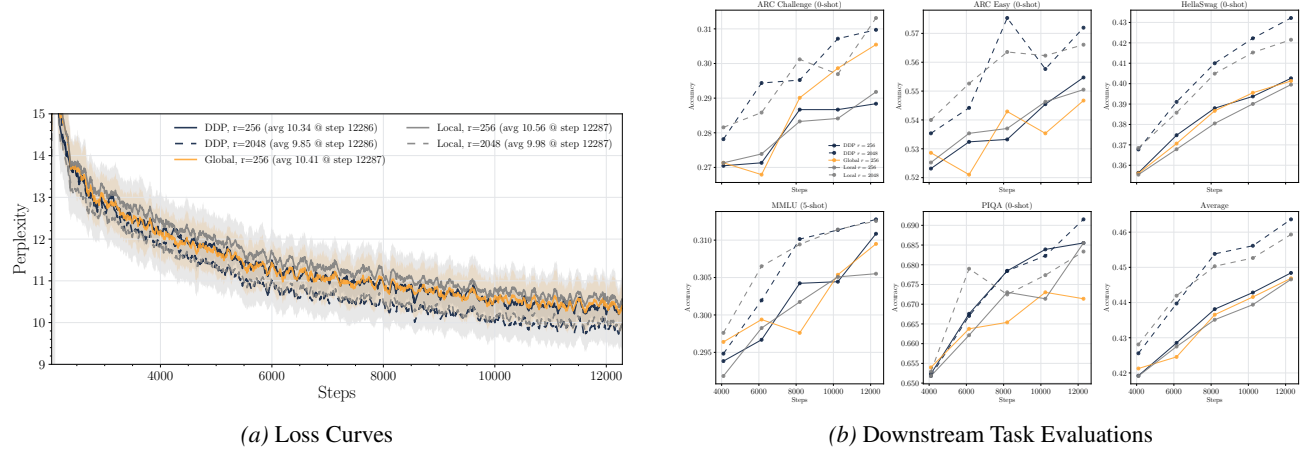


Figure 10. Comparison of LORDO and DDP at the 720M scale. Figure 10a shows that LORDO is consistent with its DDP counterpart, which is reflected in all downstream tasks. While a gap between low-rank and full-rank optimizers exists, we posit that with a longer training duration, LORDO would tend toward the performance of the full-rank DDP.

F. Extended Related Work

Memory-Efficient Optimization and Communication Compression. Significant research targets communication volume reduction by compressing the synchronization payload rather than altering the local optimization state representation. Techniques such as quantization (Alistarh et al., 2017) and sparsification (Lin et al., 2018) reduce the bits transmitted per synchronization. In LLM training, **CocktailSGD** (Wang et al., 2023) combines random sparsification, top- k selection, and quantization. **DeMo** (Peng et al., 2024) employs error feedback with top- k compression on gradients. In the federated setting, **Streaming DiLoCo** (Douillard et al., 2025) and **MuLoCo** (Thérien et al., 2025) apply compression to the pseudo-gradients exchanged between workers. **DiLoCoX** (Qi et al., 2025) integrates pipeline parallelism with a dual optimizer policy, employing low-rank compression on pseudo-gradients after local training. Similarly, **SparseLoCo** (Sarfi et al., 2025) replaces DiLoCo’s global outer momentum with a local error-feedback accumulator to enable aggressive top- k sparsification. We leave the integration of these compression techniques with our low-rank framework for future work.

Communication Mechanics of Low-Rank Updates. Beyond standard compression, distinct communication trade-offs arise depending on the specific low-rank strategy employed. In the **local** method, utilizing either low-rank quasi-hyperbolic

updates or standard updates provides a direct communication benefit, as only the low-rank matrices of the pseudo-gradient need to be transmitted. For the **global** method without quasi-hyperbolic updates, the communication benefit increases as transmitting projection matrices becomes unnecessary; however, this approach is limited to a fixed rank- r subspace, potentially causing learning stagnation. Conversely, the **global** method with quasi-hyperbolic momentum requires transmitting the full pseudo-gradient to enable the server to form a new basis. While this forfeits the intrinsic low-rank communication reduction for the gradient itself, it ensures robust subspace exploration. Crucially, this full-rank transmission remains fully compatible with other compression methods from prior work, such as quantization and sparsification, and we leave the study of this composition for future work.

Alternative Subspace Estimation Techniques. Beyond SVD (used in `Galore`) and Block Power Iteration (used in `LDAdam`), other methods exist for estimating significant gradient subspaces. **FFT-based Subspace Selection** (Modoranu et al., 2025) offers a computationally cheaper alternative using the Discrete Cosine Transform (DCT) matrix to select columns dynamically based on alignment with the gradient. `Dion` (Ahn et al., 2025) also falls into this category by enabling rank- r orthogonalization; however, it typically relies on QR decomposition, which requires execution at every step, incurring significant computational costs that scale with rank (Modoranu et al., 2025). While we primarily discuss SVD-based projections, our framework’s core contribution—handling subspace misalignment in infrequent synchronization—is agnostic to the specific estimation method. We leave the exploration of integrating these faster or alternative subspace estimators into our distributed framework for future work.

Connection to the FedOpt Framework. Our approach fits within the **FedOpt** (Reddi et al., 2021) abstraction, which generalizes Federated Averaging (FedAvg) (McMahan et al., 2017) by allowing the server (outer optimizer) to maintain its own state. **Mime** (Karimireddy et al., 2020) represents another point in this design space, using control variates to reduce client drift. Our innovation specifically modifies the *internal structure* of the client-side optimizer states (projecting them to low-rank) rather than just the aggregation logic or control variates, offering a new dimension for optimization efficiency within the FedOpt paradigm. Crucially, the underlying principle of projecting local optimizer states into a low-rank subspace is optimizer-agnostic; while we focus on adaptive methods, the framework generalizes to other stateful optimizers. The investigation of other outer optimizers or control variates within our low-rank framework is left for future work.

G. Hyperparameter Tuning and Warm-up Procedure

Below, we detail the hyperparameter tuning procedure for both `DDP` and `LORDO`. For all the non-quasi-hyperbolic experiments, we follow previous literature that establishes that learning rates transfer effectively between `DDP` and the distributed setting (Iacob et al., 2026b). This allows us to ensure that all models achieve the best performance possible in the `DDP` setting, which then transfers to `LORDO` in the non-quasi-hyperbolic case.

Given that the quasi-hyperbolic formulation is only activated following the warm-up period, although `DDP` and `LORDO` follow the same tuning methodology, we conduct independent tuning sweeps to ensure that the comparisons across `DDP` and `LORDO` were fair and consistent, given the differences in the two methods. The procedure that we implement for both methods follows the two-phase approach as per Iacob et al. (2026a). Specifically:

- i **Choosing best warm-up hyperparameters.** Both `DDP` and `LORDO` adopt the best hyperparameters for the optimizer for the pre-warm-up phase to ensure that the baselines at the warm-up cut-off are as strong as possible.
- ii **Choosing hyperparameters post warm-up.** At the end of the warm-up, both `DDP` and `LORDO` use the same model state produced by the warm-up checkpoint. Then, each method independently tunes the hyperparameters (specifically, the new learning rate η and the ω coefficient for quasi-hyperbolic momenta) to determine the optimal setting in each. This is effectively done in the stable portion of the `WSD` schedule. For both the `DDP` and `LORDO` tuning, we fix $\beta_1 = 0.999$ following warm-up phase in the case of the quasi-hyperbolic experiments.

In the case of all methods, we sweep over $\omega \in \{0.90, 0.91, 0.92, 0.93, 0.94, 0.95, 0.96, 0.97, 0.98, 0.99\}$. For the learning rates, we consider grids in increasing powers of two to find the optimal value as we show in Sections G.2 to G.4.

G.1. Findings: Ablation on Low- and Full-Rank QHM

In addition to the hyperparameter sweeps for global and `LORDO-Local`, Figure 15 provides us with an ablation across both low- and full-rank quasi-hyperbolic momentum updates for two `LORDO` variants. Focusing on `LORDO-Global`, we first

observe that adding quasi-hyperbolic momentum terms in their low-rank form does alleviate the learning stagnation. The additional gradient signal is still confined to the low-rank subspace induced by the projection matrix. This is unlike the full-rank gradient signal, which allows LORDO-Global to explore the full d dimensional representation space. Furthermore, we find that the difference between the two variants (low- and full-rank QHM LORDO-Global) decreases as the rank increases, as expected; as there is less compression, LORDO-Global can explore more dimensions within its representation.

For LORDO-Local, we observe the opposite: there is very little difference as to whether one applies the quasi-hyperbolic momentum term in its low- or full-rank form. The reason for this is that, irrespective the local optimization signal, the pseudo-gradient signal still recovers its full-rank structure following aggregation across workers. Furthermore, the full-rank variant is, at best, as performant as low-rank QHM for LORDO-Local. As such, we use low-rank QHM for LORDO-Local and full-rank QHM for LORDO-Global, respectively, throughout our experiments.

G.2. Non-Quasi-Hyperbolic Sweeps

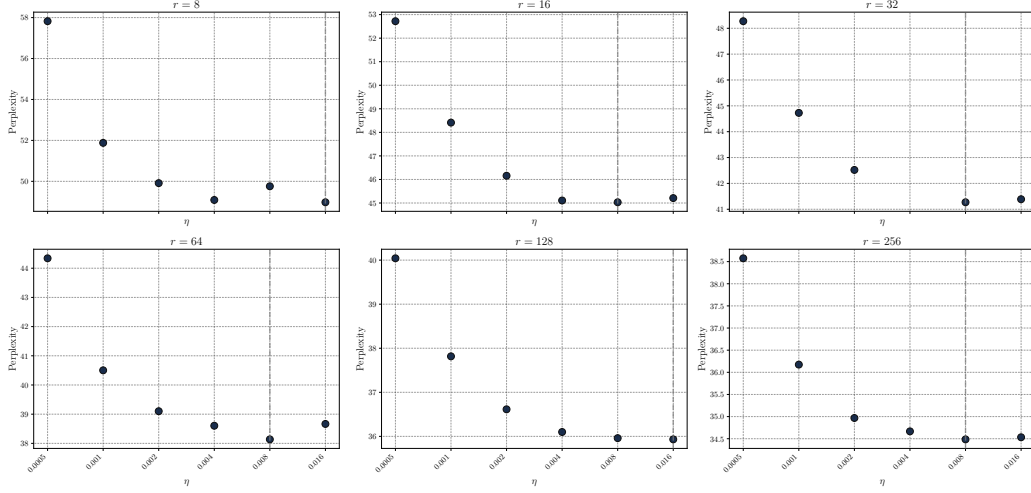
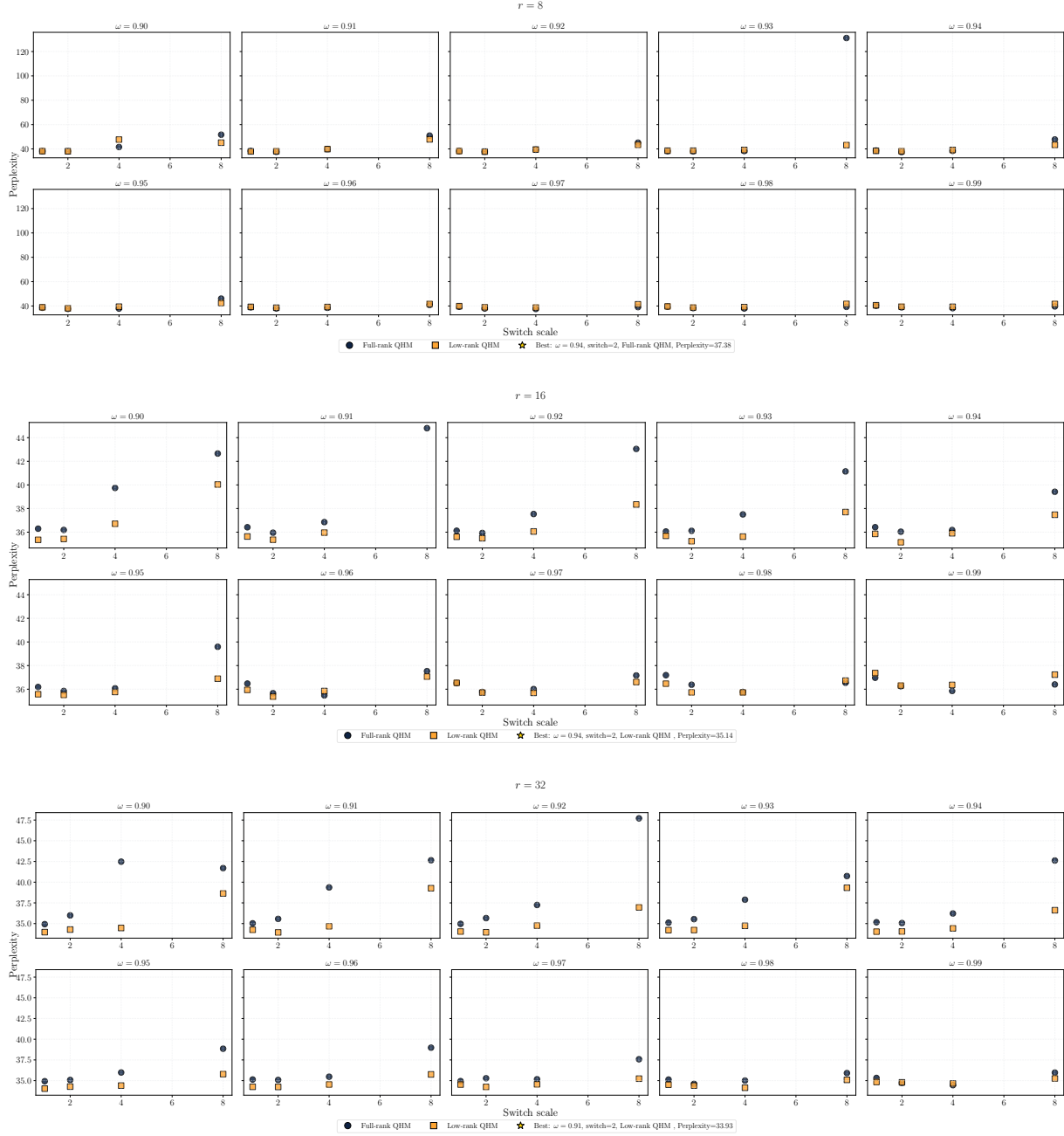


Figure 11. Hyperparameter sweep across $\eta \in \{0.0005, 0.001, 0.002, 0.004, 0.008, 0.016\}$ for 16M models to determine optimal learning rate for warmed up model training starting point.

G.3. DDP Quasi-Hyperbolic Sweeps



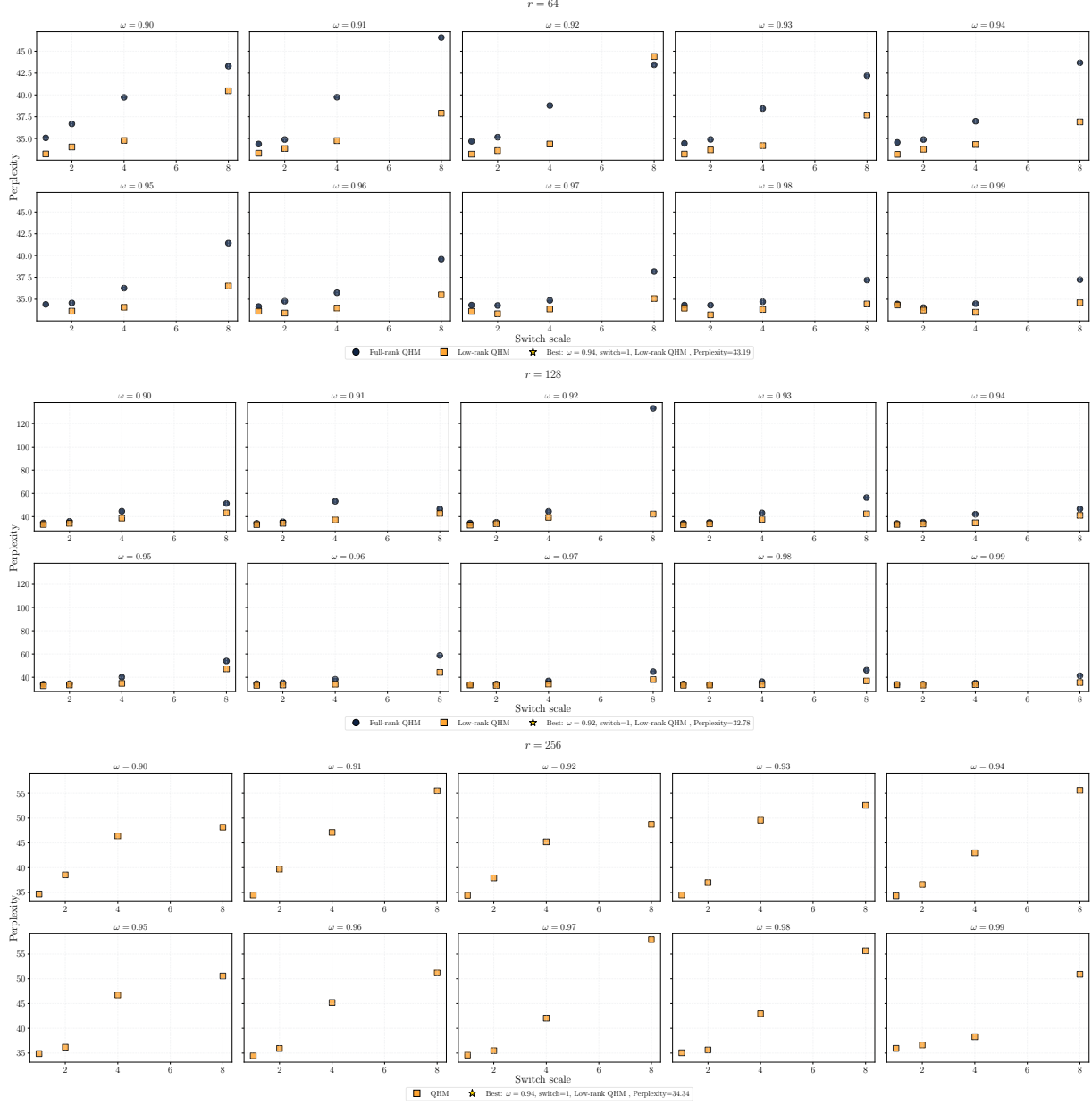
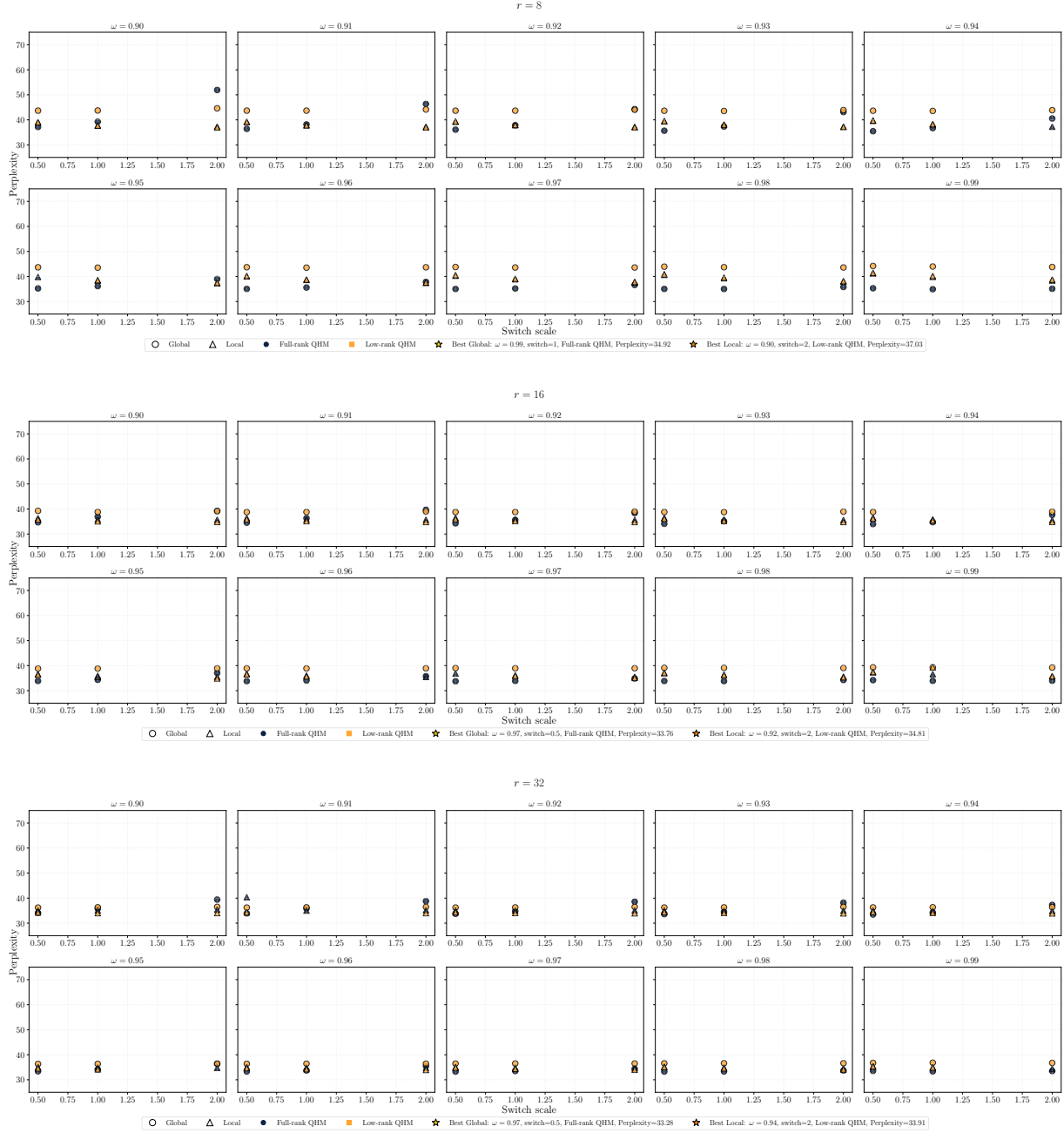


Figure 13. Hyperparameter sweep for 16M models trained with DDP, where $\beta_1 = \beta_2 = 0.999$ across $r \in \{8, 16, 32, 54, 128\}$ for combinations of $\omega \in [0.90, 0.99]$ and different multiples (switch scale) of the learning rate as per (Iacob et al., 2026a). For sweep combination, we show the effect of applying the quasi-hyperbolic formulation in its full-rank or low-rank form. Due to the approximation that the full-rank QHM method uses, it has a larger tendency to diverge quicker in regimes where it is not well-tuned, relative to the low-rank counterpart. However, in well-tuned regimes, there is little difference between the full or low-rank QHM versions, although the low-rank QHM is consistently superior. This corroborates earlier findings where our LORDO’s local variant does not benefit from a full-rank QHM formulation, unlike the global counterpart.

G.4. LORDO Quasi-Hyperbolic Sweeps



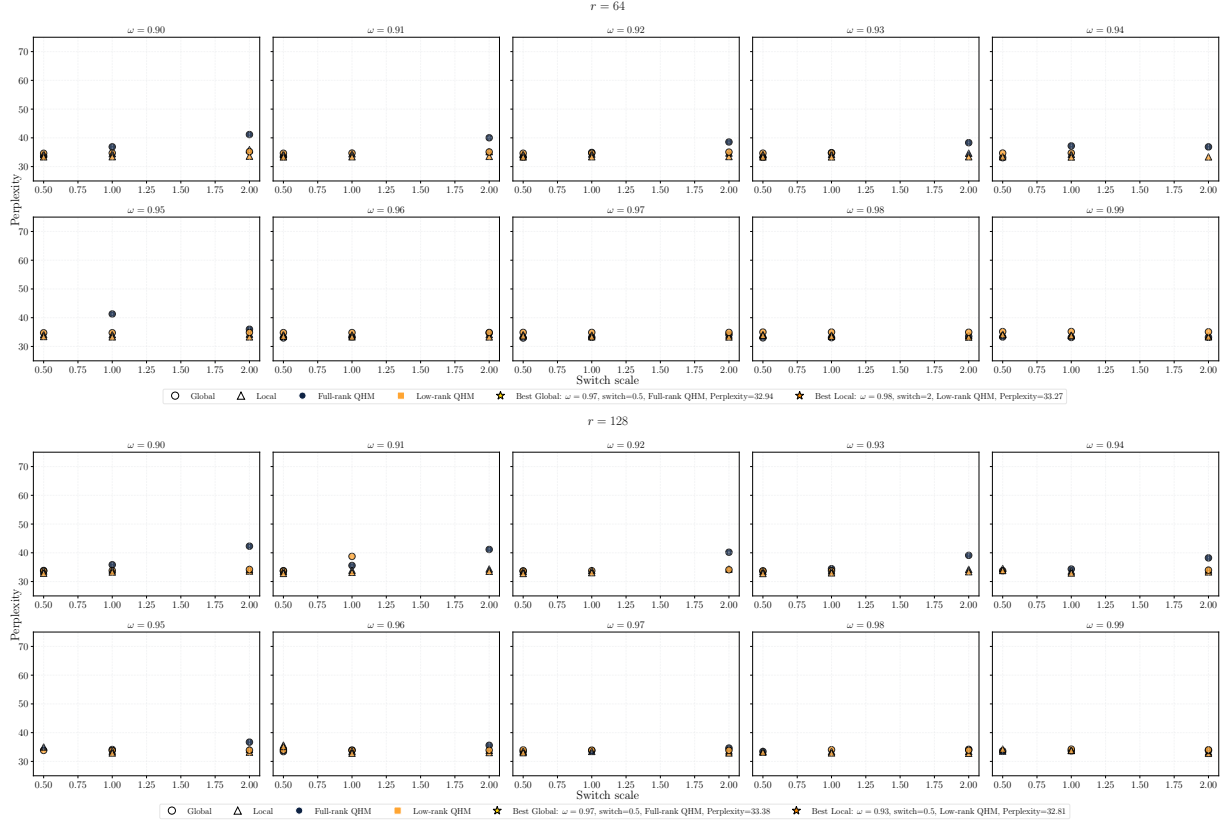


Figure 15. Hyperparameter sweep for 16M models trained with LORDO, where $\beta_1 = \beta_2 = 0.999$ across $r \in \{8, 16, 32, 54, 128\}$ for combinations of $\omega \in [0.90, 0.99]$ and different multiples (switch scale) of the learning rate as per (Jacob et al., 2026a). For sweep combination, we show the effect of applying the quasi-hyperbolic formulation in its full-rank or low-rank form. As in Figure 13, due to the approximation that the full-rank QHM method uses, it has a larger tendency to diverge quicker in regimes where it is not well-tuned, relative to the low-rank counterpart. However, in well-tuned regimes, the full-rank QHM is essential to ensuring good performance for LORDO-Global, where LORDO’s local variant does not benefit from a full-rank QHM formulation.